Remote Sensing of Environment 270 (2022) 112850

Contents lists available at ScienceDirect

Remote Sensing of Environment

journal homepage: www.elsevier.com/locate/rse

Evaluation of Sentinel-3A and Sentinel-3B ocean land colour instrument green instantaneous fraction of absorbed photosynthetically active radiation

Nadine Gobron [a,*], Olivier Morgan [a], Jennifer Adams [b], Luke A. Brown [c], Fabrizio Cappucci [a], Jadunandan Dash [c], Christian Lanconelli [a], Mirko Marioni [a], Monica Robustelli [a]

[a] European Commission, Joint Research Centre, Via Enrico Fermi, 2749 21027 Ispra (VA), Italy
[b] ϕ-lab, European Space Agency/ESRIN, Largo Galileo Galilei 1, 00044 Frascati (Roma), Italy
[c] School of Geography and Environmental Science, University of Southampton, Southampton SO17 1BJ, United Kingdom

ARTICLE INFO

Editor: Jing M. Chen

Keywords:
Green instantaneous FAPAR
OLCI
GBOV
Validation
3D-RT model
Copernicus

ABSTRACT

This article presents the evaluation of the Copernicus Sentinel-3 Ocean Land Colour Instrument (OLCI) operational terrestrial products corresponding to the green instantaneous Fraction of Absorbed Photosynthetically Active Radiation (FAPAR) and its associated rectified channels. These products are estimated using OLCI spectral measurements acquired at the top of the atmosphere by a physically-based approach and are available operationally at full (300 m) and reduced (1.2 km) spatial resolution daily. The evaluation of the quality of the FAPAR OLCI values was based on the availability of data acquired over several years by Sentinel-3A (S3A) and Sentinel-3B (S3B). The evaluation exercise consisted of several stages: first, an overall comparison of the two S3 platform products was carried out during the tandem phase; second, comparison with an FAPAR climatology derived from the Medium Resolution Imaging Spectrometer (MERIS) provided information on the seasonality of various types of land cover. Then, direct comparisons were made with the same type of FAPAR products retrieved from two sensors, the Moderate Resolution Imaging Spectroradiometer (MODIS) and the Sentinel-2 (S2) Multispectral Instrument (MSI), and with several ground-based estimates. In addition, an analysis of the efficiency of the retrieval algorithm with 3D radiative transfer simulations was performed. The results indicated that the consistency between daily and monthly S3A and S3B on a global scale was very good during the tandem phase (RMSD = 0.01 and a correlation R^2 of 0.99 with a bias of 0.003); we found an agreement with a correlation of 0.95 and 0.93 (RMSD = 0.07 and 0.09) with JRC FAPAR S2 and JRC FAPAR MODIS, respectively. Compatibility with the ground-based data was between 0.056 and 0.24 in term of RMSD depending on the type of vegetation with an overall R^2 of 0.89. Immler diagrams demonstrate that their variances were lower than the total uncertainties. The quality assurance using 3D radiative transfer model has shown that the apparent performance of the algorithm depends strongly on the type of in-situ measurement and canopy type.

1. Introduction

Remote sensing products contribute to the continuous monitoring of the Earth's surface. Within the European Union's Copernicus program, the Sentinel missions were launched with the specific objective of monitoring Essential Climate Variables (ECV) identified by the Global Climate Observing System (GCOS) (GCOS, 2016). These variables include the Fraction of Absorbed Photosynthetically Active Radiation (FAPAR), which is provided as a Level 2 land core product by the Sentinel-3 (S3) Ocean and Land Colour Instrument (OLCI) sensors at 300 m and 1.2 km, for each daily acquisition. Sentinel-3A (S3A) and its twin Sentinel-3B (S3B) were launched respectively in February 2016 and April 2018. The S3 OLCI is a direct successor to the Medium Spectral Resolution Imaging Spectrometer (MERIS) (Donlon et al., 2012), enabling continuity in the monitoring of products like green instantaneous FAPAR using the same retrieval algorithms. A series of Joint Research Centre (JRC) FAPAR algorithms have been optimised for various optical instruments such as SeaWiFS (Gobron et al., 2002),

* Corresponding author.
E-mail address: nadine.gobron@ec.europa.eu (N. Gobron).

https://doi.org/10.1016/j.rse.2021.112850
Received 16 June 2021; Received in revised form 10 December 2021; Accepted 11 December 2021
Available online 21 December 2021

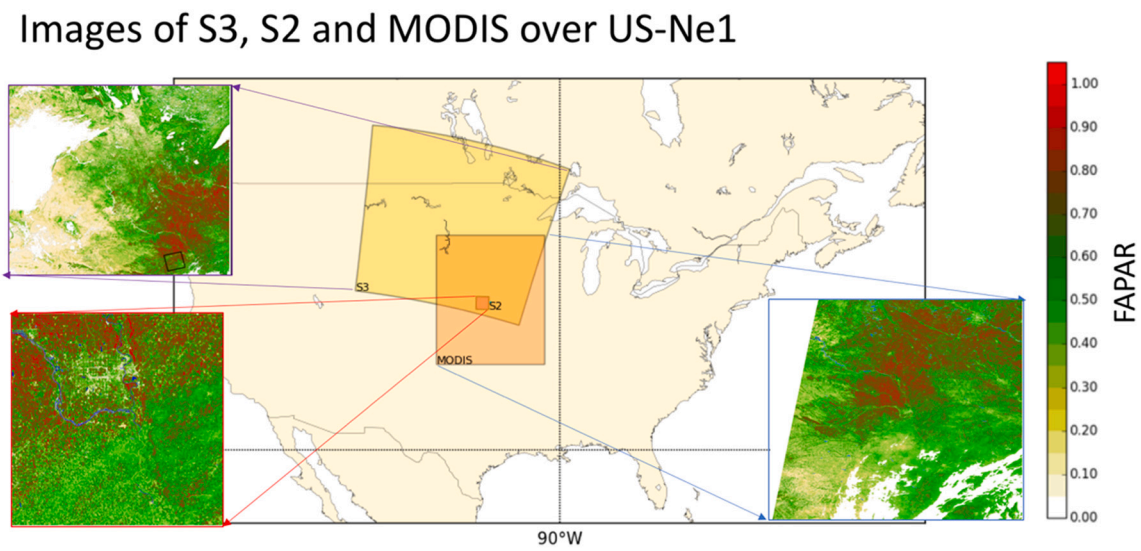

Fig. 1. Original FAPAR maps of S3/OLCI, S2/MSI and MODIS using JRC algorithm over US-Ne1 site, 12 September 2017.

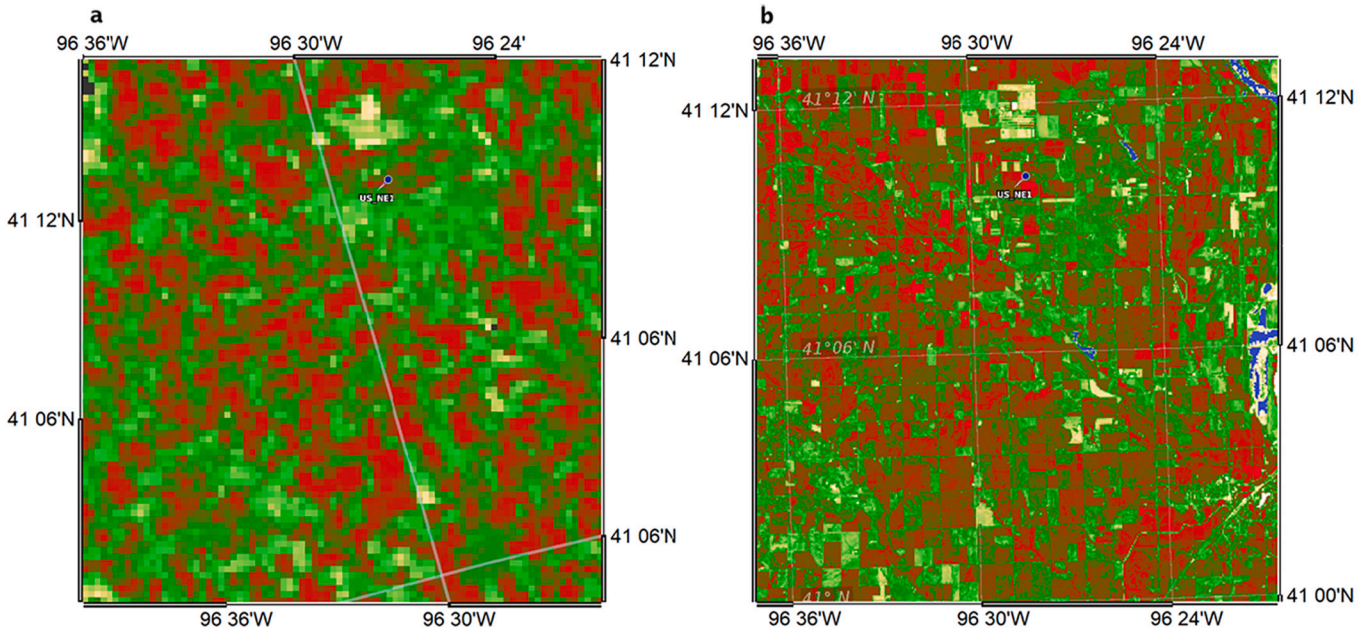

Fig. 2. a) Zoom of S3A OLCI and b) S2B MSI JRC FAPAR over US-Ne1 site.

MERIS (Gobron et al., 2004), MODerate resolution Imaging Spectroradiometer (MODIS) (Gobron et al., 2006a) and Advanced Very-High-Resolution Radiometer (AVHRR) (Gobron et al., 2019). The retrieval algorithm is based on a Look Up Table (LUT) of Bidirectional Reflectance Factors (BRFs) simulating specific sensor spectral bands and was created using the semi-discrete radiative transfer model (Gobron et al., 1997) to represent the spectral and directional reflectance of horizontally homogeneous plant canopies, as well as to compute the associated green instantaneous FAPAR values. The Second Simulation of the Satellite Signal in the Solar Spectrum (6S) atmospheric model was used to represent the atmospheric absorption and scattering effects on the measured reflectances at the top of atmosphere (Vermote et al., 1997; Kotchenova et al., 2006). The rectified reflectances correspond to the amplitude parameter of the BRF entering the Rahman, Pinty, Verstraete (RPV) parametric model (Rahman et al., 1993). They are virtual (in that they are not directly measurable in the field) spectral reflectances in which the atmospheric and angular effects are supressed. The information contained in the blue band (OLCI Band O3) is combined with that in the red and near-infrared bands (OLCI Band O10 and Band O17), traditionally used to monitor vegetation, in order to generate rectified bands at the latter two wavelengths. The rectification is done in such a way as to minimise the difference between the rectified bands and the spectral reflectances that would have been measured at the top of the canopy under identical geometrical conditions but in the absence of the atmosphere (Gobron, 2011).

Validation of remote sensing land products encompasses different frameworks and steps including at its simplest, quality control, benchmarking against third-party data and comparison against ground-based reference data measurements (Loew et al., 2017). Land products from S3 OLCI sensors have already been compared against third-party products, such as National Aeronautics and Space Administration (NASA) MODIS, Visible Infrared Imaging Radiometer Suite (VIIRS), Copernicus Global Land Service (CGLS), Multi-angle Imaging Spectro Radiometer (MISR), Earth Polychromatic Imaging Camera (EPIC) at 0.2° together with Solar-

Table 1
S3VT Validation sites.

Code	Latitude (°N+)	Longitude (°E+)	MGRS[a]/UTMREF	Land Cover Type	Reference
DE-Geb	51.1001	10.9143	32UPB34036269	Croplands	Truckenbrodt and Baade, 2018
DE-Rod	50.8300	11.7700	32UPB95063457	Croplands, Evergreen Needleleaf Forest, Deciduous Needleleaf Forest	Truckenbrodt and Baade, 2018
DE-Thf	50.5730	10.8450	32UPB30640396	Mixed Forest	Truckenbrodt and Baade, 2018
IT-Cat	37.2785	14.8832	33SVB89652577	Croplands (Orange)	Vuolo et al., 2012
IT-Isp	45.8128	8.6345	32TMR71537329	Mixed Forest	Gruening et al., 2012
IT-Sro	43.7278	10.2844	32TPP03444244	*Pinus Pinea*	Gruening et al., 2012
IT-Tra	37.6455	12.8527	33SUB10566865	Croplands (Vineyards and olive trees)	Vuolo et al., 2012
RU-Bol	57.05	93.3700	46VEJ22442301	Mixed Forest	n/a
RU-Kul	52.5611	80.7085	44UMD80242348	Cultivated Areas	n/a
SP-Ala	38.4515	−1.0645	30SXH68885769	Semi-arid Mediterranean	Lopez-Baeza et al., 2013
SP-Val	39.5207	−1.2925	30SXJ46767595	Semi-arid Mediterranean	Lopez-Baeza et al., 2013
UK-NFo	50.8498	−1.5740	30UXB00378341	Natural deciduous forest	Brown et al., 2019
US-Ne1	41.1650	−96.4766	14TQL11706015	Croplands (Maize)	Gitelson et al., 2014 Suyker, 2021
US-Ne2	41.1648	−96.4701	14TQL12246014	Croplands (Irrigated Maize Soybean rotation)	Gitelson et al., 2014 Suyker, 2021
US-Ne3	41.1797	−96.4396	14TQL14746186	Croplands (Rainfed Maize Soybean rotation)	Gitelson et al., 2014 Suyker, 2021

[a] Military Grid Reference System - Sentinel-2 Tiles.

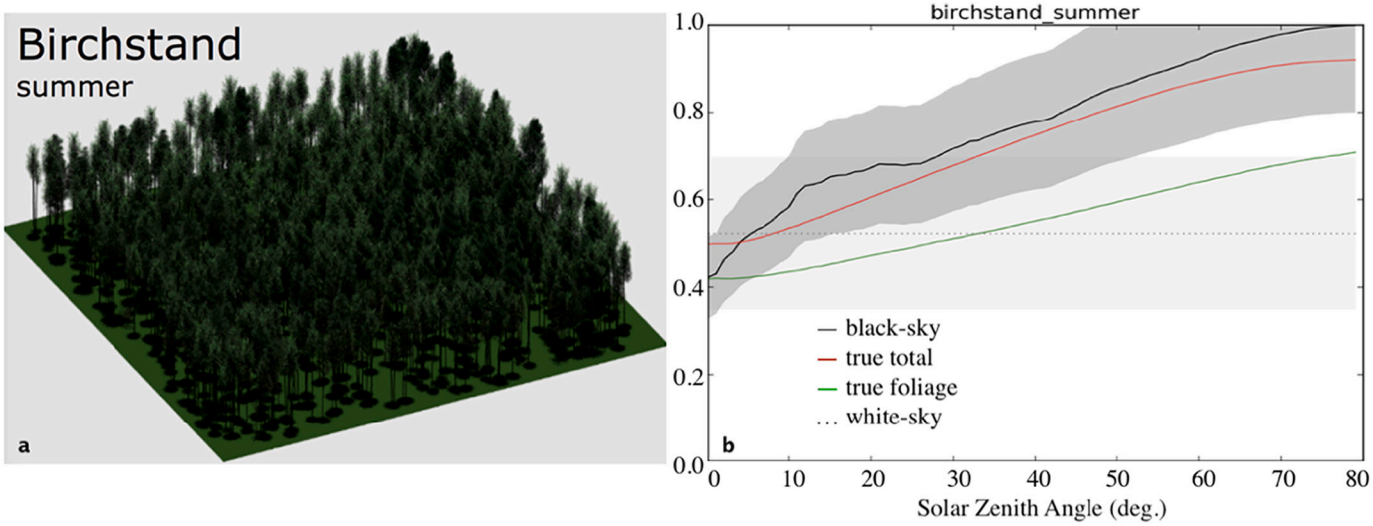

Fig. 3. a) View of the Järvselja-2 (*birchstand summer)* scene and b) the virtual values of total black-sky and white-sky the DHP compared to the 'true' values (total and foliage only) using 3D-RT modelling.

Induced chlorophyll Fluorescence (SIF) space products (Zhang et al., 2020). The authors found that OLCI FAPAR had the best relationships with TROPOspheric Monitoring Instrument (TROPOMI) nSIF740 (e.g. solar angle normalised SIF at 740 nm), Orbiting Carbon Observatory-2 (OCO-2) nSIF757, and airborne (Chlorophyll Fluorescence Imaging Spectrometer, CFIS) nSIF755 with a coefficient of determination, R^2, of 0.79 ± 0.17 on a global scale. APAR calculated with OLCI FAPAR also showed the best results ($R^2 = 0.79$) with in situ Gross Primary Production (GPP) over 25 flux towers (Zhang et al., 2020). This is mainly due to the definition of OLCI FAPAR products as it represents the instantaneous (direct) green (foliage) component. Alternative FAPAR retrieval algorithms were developed for Sentinel-2 such the one implemented in Science Toolbox Exploitation Platform (SNAP) (Weiss and Baret, 2016) that used surface reflectance data. Validation of these products was done in Putzenlechner et al. (2019) and the authors found high discrepancies of absolute FAPAR values, ranging from 13 to 25% over three forests. Brown et al. (2021a) proposed a modified version for which only Leaf Area Index (LAI) were compared against in-situ data.

Both SeaWiFS and MERIS FAPAR products, using the same OLCI retrieval algorithm, have been already validated against third-party products and in-situ ground-measurements. The results indicated that the impact of top-of-atmosphere radiance uncertainties on the operational MERIS FAPAR products accuracy was expected to be at about 5–10% whereas agreement with the ground-based estimates of the Fraction of Intercepted PAR (FIPAR) over different canopy types was achieved within ±0.1. An evaluation exercise was also performed by direct comparison, by grouping available field information into broad categories representing different radiative transfer regimes. This strategy facilitated the interpretation of the results since various levels of difficulty and sources of uncertainty associated with the radiative sampling of different types of vegetation canopies was shown in (Gobron et al., 2008). In recent years, major progress has been made in 3D-Radiative Transfer (RT) canopy modelling for both in-situ and space products validation purposes such as the sampling strategy and upscaling processes (Adams et al., 2016; Calders et al., 2018).

In this article, we first compare S3A and S3B during the tandem phase at the global scale using daily and monthly products at 1.2 km; then we benchmark them against MERIS climatology, MODIS and Sentinel-2 Multispectral Instrument (MSI) JRC FAPAR over various Sentinel-3 Validation Team (S3VT) local sites (Gobron et al., 2013) that cover different vegetation types. Finally, direct comparison against ground-based data is carried out, and we perform an algorithm

Table 2
Ground-based observation for validation Land Product-4 sites.

ID	Name	Latitude (°N+)	Longitude (°E+)	IGBP
US-BAR	Barlett Experimental Forest	44.0639	−71.2873	Mixed Forest
US-BLA	Blandy Experimental Farm	39.0603	−78.0716	Cropland
US-CPE	Central Plains Experimental Range	40.8155	−104.746	Grassland
US_DEL	Dead Lake	32.54172	−87.80389	Evergreen Broadleaf
US-DSN	Disney Wilderness Preserve	28.125	−81.4362	Woody Savanna
PR-GUA	Guanica Forest	17.9696	−66.8687	Evergreen Broadleaf
US-HRV	Harvard Forest	42.5378	−72.1715	Mixed Forest
US-JER	Jones Ecological Research Center	31.1948	−84.4686	Cropland
US-JOR	Jornana	32.5907	−106.843	Open Shrubland
PRI_LAJ	Lajas Experimental Station	18.02125	−67.0769	Grassland
US-MOA	Moab	38.2483	−109.388	Grassland
US-NRF	Niwot Ridge Mountain Research Station	40.0542	−105.582	Evergreen Needleleaf
US-STE	North Sterling	40.4619	−103.029	Grassland
US-ORN	Oak Ridge	35.9641	−84.2826	Cropland
US-ONA	Onaqui Ault	40.1776	−112.452	Grassland
US-OSB	Ordway Swisher Biological Station	29.6765	−82.0091	Woody Savanna
US-SCB	Smithsonian Conservation Biology Institute	38.8929	−78.1395	Deciduous Broadleaf
US-SER	Smithsonian Environmental Research Center	38.8901	−76.56	Cropland
US_SRE	Santa Rita	31.91068	−110.83549	Closed Shrubland
US-SLS	Steigerwalt Land Services	45.5089	−89.5863	Mixed Forest
US-TAL	Talladega National Forest	32.9505	-87.3933	Mixed Forest
US-UND	Underc	46.2339	−89.5372	Mixed Forest
US-WOO	Woodworth	47.1282	−99.24414	Cropland

Table 3
Validation sites from AMMA-CATCH and direct database.

Name	Latitude (°N+)	Longitude (°E+)	Vegetation Type	Reference
TARA	15.2301	−1.5833	Open Woody Savannah	Mougin et al., 2014
HOMBORI-HONDO	15.3224	−1.6983	Open Shrub Savannah	
KELMA	15.2189	−1.5657	Acacia Forest	
AGOUFOU	15.3393	−1.4841	Open Woody Savannah	
LIRIA	39.7519	−0.7005	NeedleLeafForest	Garrigues et al., 2008
BARRAX-LASTIESAS	39.0543	2.1006	CropLand	
MONCADA	39.5204	−0.3869	CropLand	

Table 4
QA4ECV validation sites. Aerosol models are those hardcoded in the 6S RT model.

Site	Latitude (°N+)	Longitude (°E+)	Scene	Aerosol Model
Järvselja-1*	58.313	27.297	Pine Stand	Continental
Järvselja-2*	58.277	27.296	Birch Stand	Continental
Ofenpass*	46.663	10.230	Pine Stand	Continental
Lope	−0.169	11.459	Tropical Forest	Biomass Burning
Nghotto	3.867	17.300	Tropical Forest	Biomass Burning
Zerbolo*	45.295	8.877	Short Rotation Forest (Poplar)	Continental
Thiverval-Grignon	48.850	1.966	Wheat	Continental
Wellington*	−33.600	18.933	Citrus Orchard	Maritime
Skukuza	−25.0207	31.497	Savannah	Biomass Burning
Janina	−30.077	144.136	Shrub land	Desert

* The corresponding scenes are available on RAMI web site (WWW2, 2021; Widlowski et al., 2015).

verification using spectral simulations from the JRC virtual laboratory. Discussion and conclusions end the paper.

2. Method and data sets

2.1. Space FAPAR data

From June 2018 to October 2018, S3A and S3B were flown in tandem mode, i.e., with a 30 s separation, to enable detailed understanding of the similarities and differences between the instruments contained on each platform (Lamquin et al., 2020a). Therefore, we performed a comparison at global scale to ensure the compatibility of FAPAR values as retrieved from S3A and S3B OLCI data. Even with only a 30 s difference, there was no guarantee that both satellite footprints were at the exact same geolocation; the results were firstly analysed using a spatial average over 3 × 3 pixels to reduce any co-geolocation issues for two single days and secondly from June to October 2018 with daily and monthly products.

Daily spectral measurements from MODIS and S2 MSI were used to support this analysis. Since 2002, MODIS has provided measurements in the red and near-infrared bands at 250 m spatial resolution, whereas those in the blue band are available at 500 m. Gobron et al. (2006a) already designed a retrieval algorithm at 250 m comparable to OLCI FAPAR's one and that has been used for MERIS validation purposes. Since 2016, we also had access to S2A and S2B data, in the form of optical spectral measurements with the MSI at 10 m, 20 m and 60 m (Drusch et al., 2012). The S2 MSI JRC FAPAR was designed and produced at 60 m to be used instead of, or together with, ground-based measurements. Fig. 1 illustrates the three maps of FAPAR from these sensors over the Nebraska site (US-Ne1) in the USA on the 12 September 2017. To benchmark them, all products were resampled into the WGS 84 latitude/longitude grid projection using a nearest-neighbour approach (see Fig. 2).

The MERIS FAPAR dataset over 2003–2011 at 300 m (MERIS third-reprocessing) was used to define the climatology of various land cover types and compared with OLCI FAPAR values. The climatology was performed on selected S3VT sites which are in stable and controlled conditions concerning the land cover type. As we used MERIS daily data, some outliers were still present due to the contamination of remaining

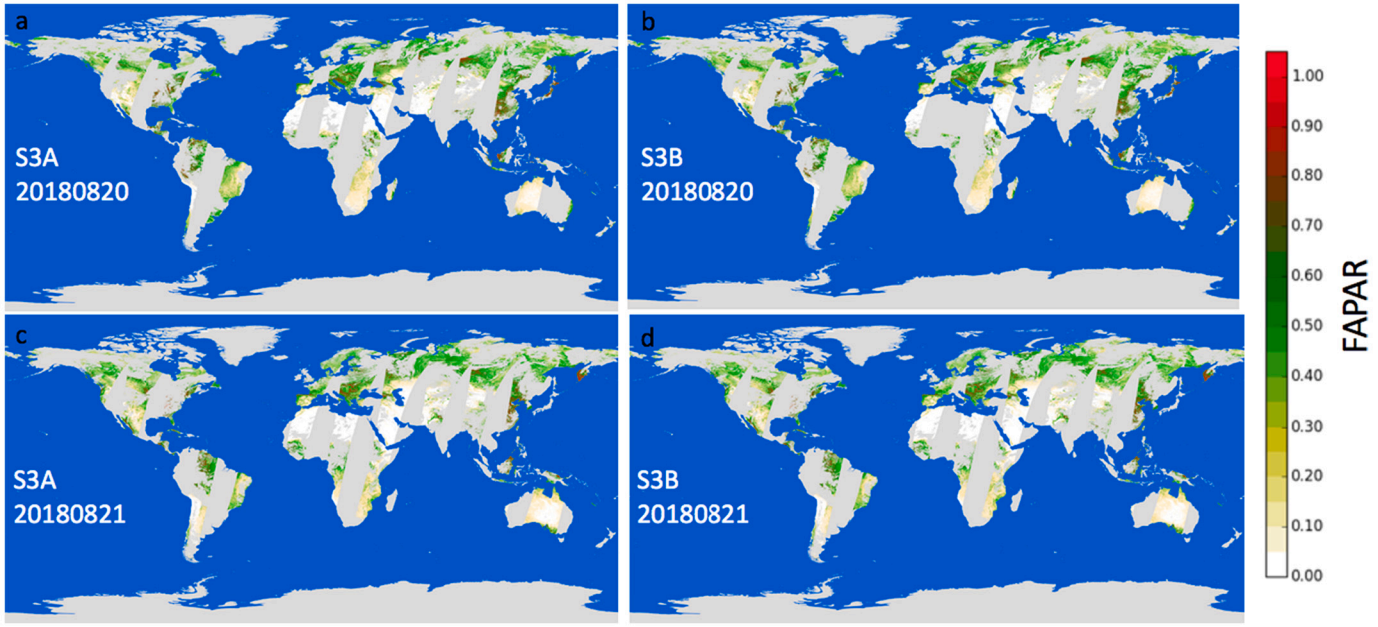

Fig. 4. Global Maps of FAPAR with a-(c) S3A; b-(d) S3B OLCI on 20(−21) August 2018.

cloud or cloud shadow, even in the climatology, data were therefore smoothed using a temporal running average over 15 days. All the comparisons with EO products were done over the core validation sites selected by the S3VT (Gobron et al., 2013) (see Table 1). They represent several land cover types with potential access to time series of ground-based data.

2.2. Ground-based data

In 2016, a specific validation campaign over the New Forest site, UK-NFo, provided estimates of FAPAR that could be directly compared to OLCI FAPAR. Details of this campaign can be found in Brown et al. (2019). In summary, various Digital Hemispherical Photographs (DHPs) have been taken at 8 different dates providing 5 measurements in 9 Elementary Sampling Unit (ESUs) covering an area of 1.2 km × 1.2 km. The images were then analysed by the Can-Eye software (Weiss and Baret, 2014) to extract the instantaneous black-sky FAPAR (FAPAR_BS), the daily integrated black-sky FAPAR and white-sky FAPAR (FAPAR_WS) over all ESUs. These ground-based data cannot directly infer the exact same physical quantity as OLCI FAPAR because they provided the total absorption and not just the foliage absorption. Therefore, we evaluated the expected bias using our virtual laboratory (see next section) for the Järvselja-2 site, representing the similar canopy as the New Forest, e.g. the *birchstand summer* scene, as illustrated in Fig. 3. The difference between the total and the 'true' foliage values provided information on the expected bias between the two definitions of FAPAR, i.e. between typical in-situ measurements and OLCI products. For the validation against S3 OLCI FAPAR, the DHP-FAPAR (black-sky) calculated at 10.50 AM was therefore bias corrected using our 3D-RT results. This has been done by removing the difference between true total and true foliage values to DHP.

More recently, the Ground-Based Observations for Validation (GBOV) of Copernicus Global Land Products service delivers up-scaling data for validation of various land variables (Brown et al., 2020, WWW1, 2021). The raw data were measured with the DHP methodology providing FIPAR values and then up-scaled to provide data at 300 m over 23 sites, covering different land cover types (see Table 2). Values represent the total amount of intercepted radiation, even though DHP images were acquired both up and down for understory and overstory sites. In theory, it would be also possible to distinguish between the foliage and woody elements of the canopy such as stems and branches, allowing the ground-based to be corrected. Gobron et al. (2006b) demonstrated that expected differences between FIPAR and FAPAR are up to 0.1 happen over very bright backgrounds, they can be neglected in the overall uncertainty budget under normal conditions (i.e. where a vegetated understory is present). We were not able to make any correction for GBOV data as this would require intensive measurements needed for the 3D-RT simulations. These up-scaled reference data, known as Land Products (LPs), also include quality flags and uncertainties. The comparisons were performed using 3 × 3 pixels during the growing season when 100% coverage of valid value was available for both space and up-scaling data. A maximum two days' difference between acquisitions of OLCI and LPs was imposed.

In addition to DHP derived data, FAPAR was inferred over three agricultural FLUXNET sites (US-Ne1, US-Ne2 and UN-Ne3) located at the Lincoln Agricultural research and Development Centre near Mead (NE, USA) (Gitelson et al., 2014; Viña and Gitelson, 2005). These measurements were performed with Li-Cor quantum sensors that collect hourly measurements of PAR components as 1) incoming at top-of-canopy, 2) reflected by the canopy and soil, 3) transmitted through the canopy and 4) reflected by the soil. All daily values of radiation were then inferred by integrating the hourly data during the day when incoming PAR exceeded 1 μmol/m2/s. During the vegetative stage, the total FAPAR increase coincided with the increase of canopy green LAI. However, it remained insensitive to the decreases in crop greenness as both photosynthetic and non-photosynthetic components were intercepting radiation. Therefore, to obtain a measure of the FAPAR absorbed only by the photosynthetic component of the vegetation, a correction was applied to provide the foliage FAPAR using green LAI destructive measurements (Gitelson et al., 2003). The absorption PAR for only green elements, i.e., $FAPAR_{green}$, were obtained with the following correction for which LAI_{green} and LAI_{total} have been measured through a destructive determination technique:

$$FAPAR_{green} = FAPAR_{total} \frac{LAI_{green}}{LAI_{total}} \quad (1)$$

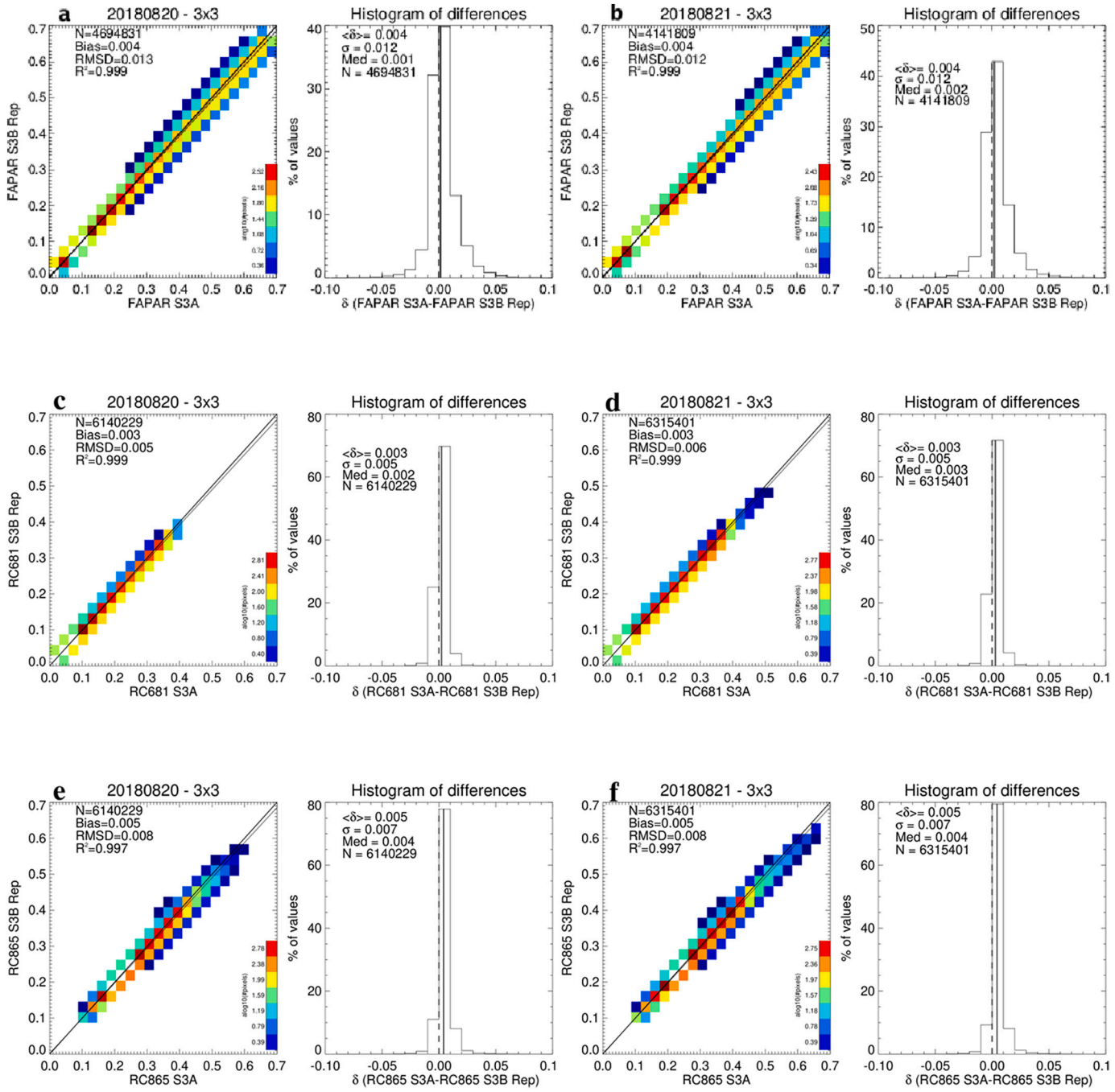

Fig. 5. Scatter-plots between S3A and S3B products on the 20 August 2018 and the 21 August 2018 for the FAPAR (a-b), rectified spectral reflectance at 681 nm (c-d) and at 865 nm (e-f) at global scale.

These ground-based measurements were therefore more suitable for the FAPAR land products validation as they better represented the same physical quantity, e.g. absorption by green leaves, but they were not upscaled as these sites are approximately 60-ha fields (Gitelson et al., 2014; Chernetskiy et al., 2017).

Since 2016, ground-based for EO validation purposes were available only over few geographical zones. The AMMA-CATCH project (Galle et al., 2018) measured both diffuse and direct values over 4 stations in West Africa (e.g. in Mali) covering 3 types of vegetation types (see Table 3). These measurements were derived from DHP images and provided an estimation of direct and diffuse total FIPAR with a difference of 5% when compared to PAR sensors, having themselves an accuracy of 10% (Mougin et al., 2014). However, these data were not upscaled to match the actual OLCI spatial resolution. In addition, we found only four single match-up within the CEOS LPV Direct 2.0 database (Garrigues et al., 2008) over two crop sites and one needle leaf forest in Europe (see Table 3). The values represent an average value over the 3 $\times$ 3 km^2 area. Any correction were applied to these data as no information on structural and spectral canopy properties were available.

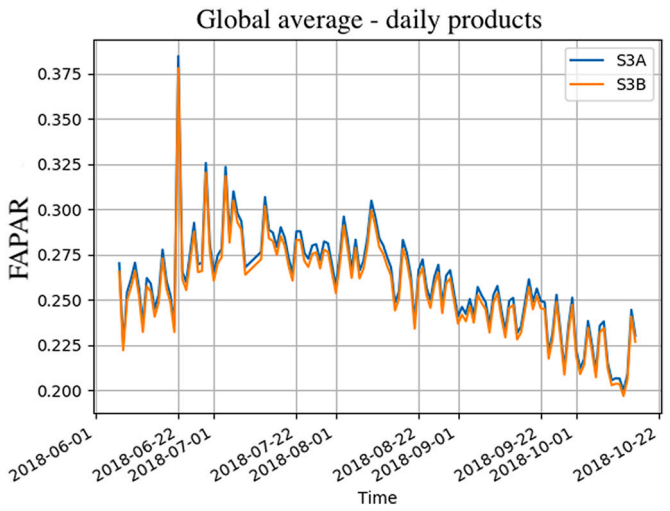

Fig. 6. Time series of global average of FAPAR from S3A (blue line) and S3B (orange line) from June to October 2018. (For interpretation of the references to colour in this figure legend, the reader is referred to the web version of this article.)

Table 5
Benchmark statistic between monthly FAPAR products from S3A and S3B in 2018.

	Slope	Intercept	R^2	RMSD	Bias
June	0.973	0.003	0.993	0.016	0.004
July	0.976	0.003	0.995	0.016	0.003
August	0.975	0.003	0.994	0.017	0.004
September	0.973	0.003	0.995	0.015	0.003
October	0.973	0.004	0.992	0.018	0.003

2.3. Virtual laboratory

The FAPAR retrieval algorithm was applied with a single-pixel based processor using as input data the simulated OLCI TOA BRFs over Quality Assurance for Essential Climate Variables (QA4ECV) validation sites. These simulations were performed during the QA4ECV project (European Union FP7 grant No.: 607405; Lanconelli et al., 2018). The JRC FAPAR values were evaluated against the 'true' value associated to the FAPAR computed by the 3D RT model Raytran (Govaerts and Verstraete, 1998) considering different physical definitions: total absorption 2-flux and 4-flux methods (representing ground-based protocols), and absorption by only the foliage component. The 2-flux and 4-flux are obtained by combining the downwelling and upwelling PAR fluxes at the top and bottom of the canopy as detailed in Widlowski (2010, AFM) such as:

$$FAPAR_{2\_flux} = 1. - \mathrm{T} \tag{2}$$

$$FAPAR_{4\_flux} = 1. - T + aT - R \tag{3}$$

where T is the transmitted flux at bottom of canopy (BOC), R is the reflected flux at BOC (i.e. the surface reflectance) and a the albedo at the TOC. The upwelling and downwelling PAR flux measurements were simulated over a matrix of 180 × 180 × (h/50 cm) at 50 cm horizontal and vertical resolution within the canopy. As the 3D ray tracing model allows to trace photon lifetime, the definition of reference value is based on the count of photons absorbed only by leaves for assessing the foliage absorption, i.e. '*abs_fol*'. The BOC level is fixed to 50 cm in all scenes.

Table 4 lists the QA4ECV virtual validation sites that cover different vegetation types. For each site, 3D scenes were developed and used in a 3D-RT model coupled with the atmospheric model to simulate OLCI sensor data in the blue, red and near-infrared. The ray tracing canopy model was coupled with the 6S model and the simulations were performed using the MODIS Aerosol Optical Depth (AOD) from the MOD08 and MYD08 D3 products over an area of 1° × 1° containing each site geographical coordinates (Levy et al., 2015). The water vapour (g/cm^2) and ozone column contents (cm − atm equivalent to DU/1000) that are the main absorbing gases in the near-infrared and visible (ozone Chappuis) spectral region, respectively were obtained from the actual OLCI Land 1 products that come from the European Centre for Medium-Range Weather Forecasts (ECMWF) data. The aerosol model adopted for each site was selected according to geographical location considering the predominant air mass advections (see Table 4). The actual geometry for both illumination and viewing angles was used to run the simulations and the OLCI FAPAR algorithm was then applied using the pixel-based process.

3. Results

3.1. S3A and S3B comparison

S3A and S3B FAPAR maps at 1.2 km for the 20 and 21 August 2018 are displayed in the top and bottom panels of Fig. 4, respectively. The corresponding scatter-plots are shown in Fig. 5.

We report the number of points which have been used, as well as the RMSD (equal to 0.012) with a bias of 0.004 and correlation of 0.999. These results indicate that S3A and S3B OLCI FAPAR products provide almost identical values, and that these twin sensors, which double the frequency of FAPAR data acquisition, can be confidently used interchangeably. The rectified spectral reflectance scatter-plots are displayed for both spectral bands at 681 nm and 865 nm with RMSD equal to 0.005 and 0.008, and a bias of 0.003 and 0.005, respectively. Rectified channels represent the spectral values that are decontaminated from atmospheric and angular effects and used as inputs for the FAPAR calculations.

In addition to these two specific days, we also compared the global average of daily FAPAR between the two platforms as shown in Fig. 6. The blue and orange curves correspond to S3A and S3B FAPAR, respectively. The global average was made using only for valid and common pixels. One note that S3A values are slightly greater that the ones from S3B, but with a systematic and very small bias as confirmed when comparing monthly products (see Table 5).

3.2. MERIS climatology

The MERIS climatology is plotted together with Sentinel-3A daily products time series over SV3T sites corresponding to various land cover types. The running average period is 15 days for both the OLCI datasets and the MERIS climatology over 2003–2011. The six crop phenology profiles show that the seasonality of OLCI overlaps well with the MERIS climatology, except over IT-Cat and DE-Geb (see Fig. 7e and Fig. 7f). Panels a, b and c illustrate the typical crop evolution over the US-Ne sites, with the start of growing season in May up to the peak in August and the senescence phase at the end of summer. We can notice that, over US-Ne2 site (Fig. 7b), a small-time lag exists between each annual OLCI FAPAR time series and the climatology; and 2019 is late in comparison to previous years, which may be due to different climatic conditions. The FAPAR profile over IT-Cat contains a maximum peak at the end of September 2018 due to heavy rain, meaning that vegetation at lower levels grew more than usual (Fig. 7e). The fact that, over DE-Geb, all seasonal features are different compared to the climatology is mainly due to the rotation of different crops (Truckenbrodt and Baade, 2018). These features were confirmed using alternative space products (not shown here).

The annual profiles over several forest types provide different climatology patterns that are well represented by OLCI FAPAR time series (see Fig. 8). However, we can notice that over DE-THF the levels measured by OLCI appear to be higher than the climatology ones

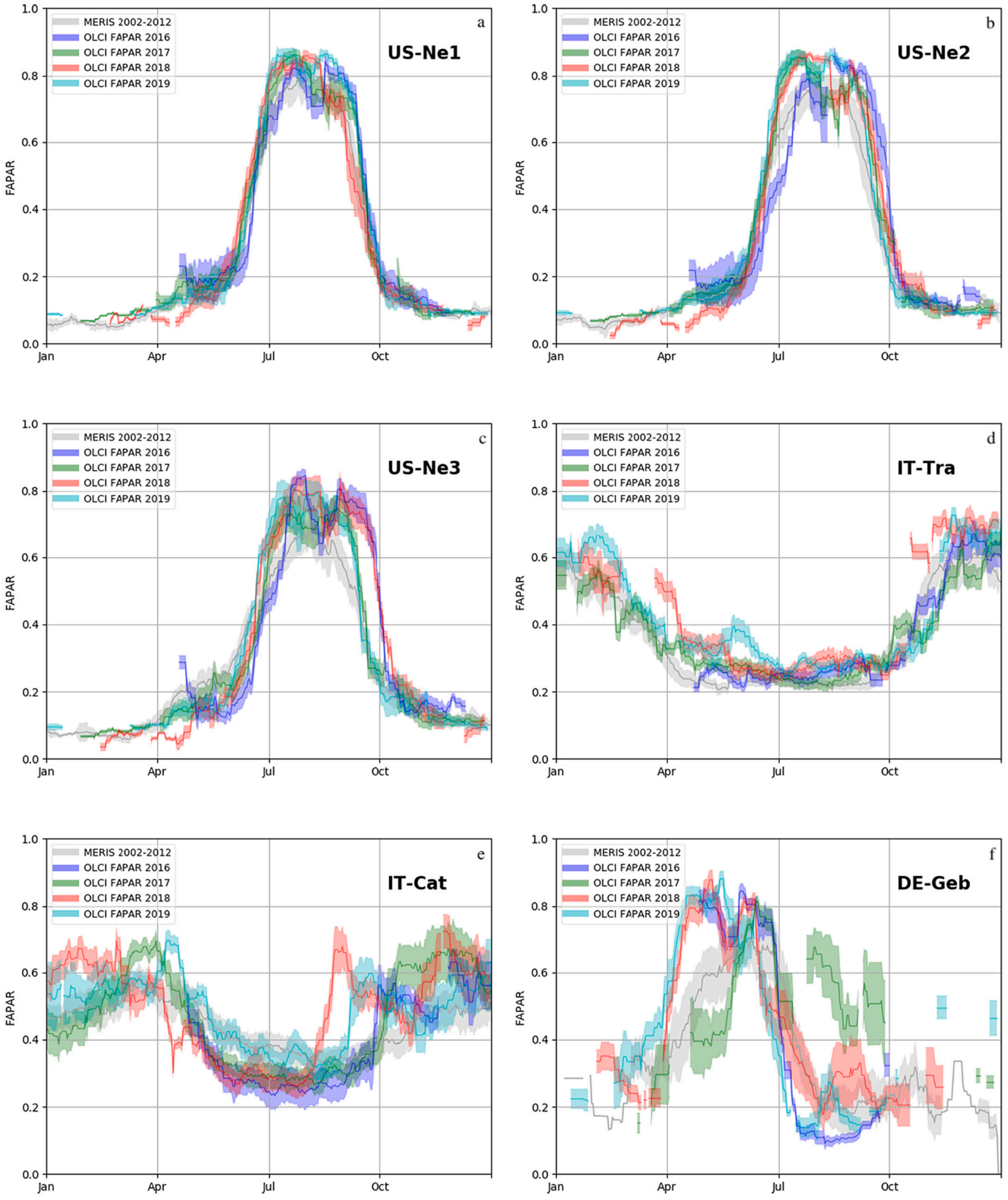

Fig. 7. Climatology of MERIS FAPAR over 2003–2011 (grey shadow) and daily S3A OLCI products in 2016 (blue), 2017 (green), 2018 (red) and 2019 (light blue) over S3VT croplands sites. The colour shades represent the spatial deviation within 3 × 3 pixels. (For interpretation of the references to colour in this figure legend, the reader is referred to the web version of this article.)

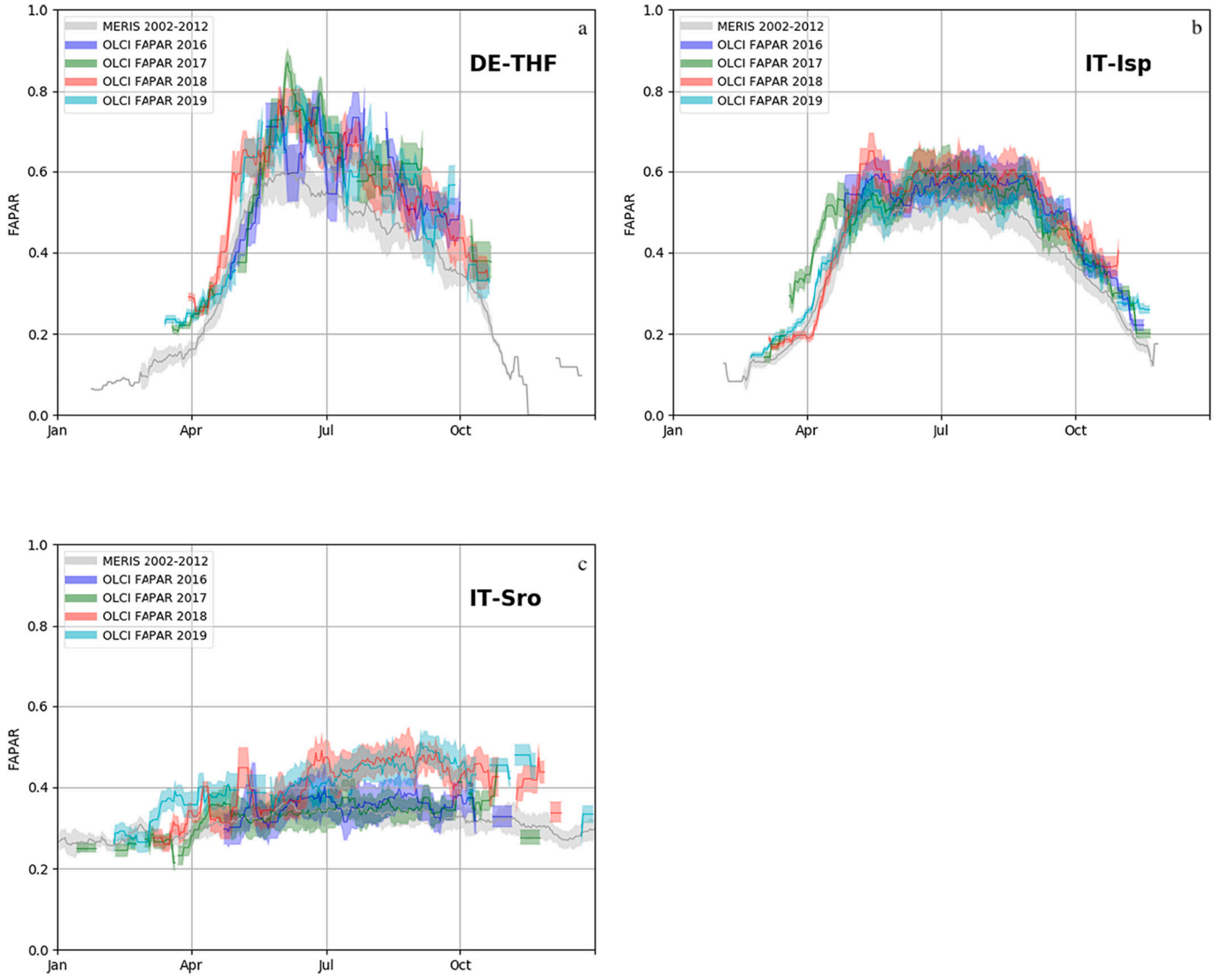

Fig. 8. Climatology of MERIS FAPAR over 2003–2011 (grey shadow) and daily OLCI products in 2016 (blue), 2017 (green), 2018 (red) and 2019 (light blue) over S3VT forests. (For interpretation of the references to colour in this figure legend, the reader is referred to the web version of this article.)

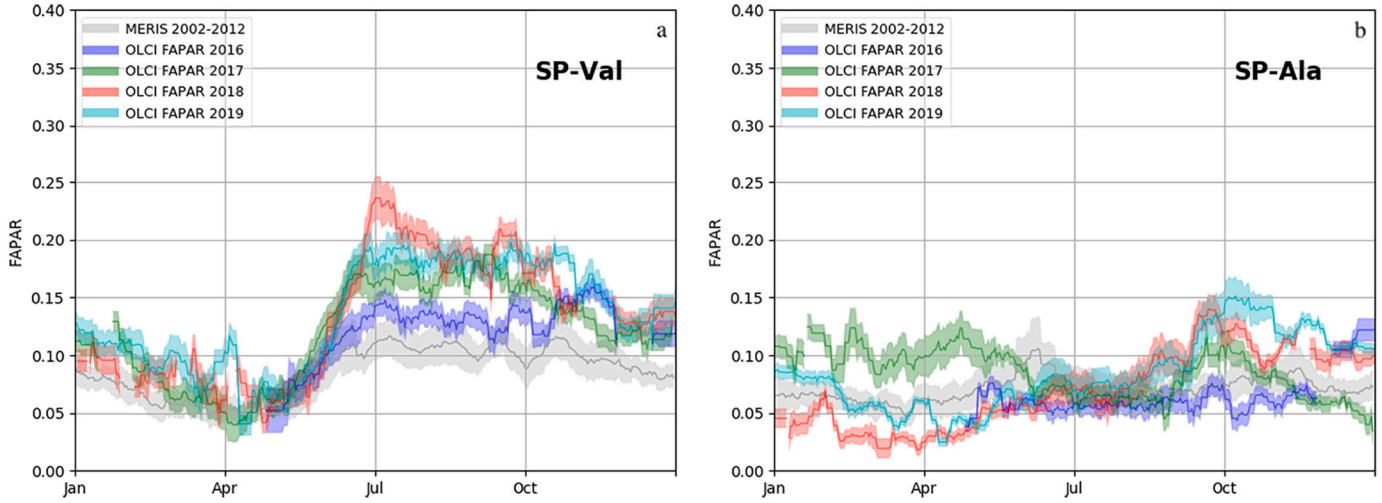

Fig. 9. Climatology of MERIS FAPAR over 2003–2011 (grey shadow) and daily OLCI products in 2016 (blue), 2017 (green), 2018 (red) and 2019 (light blue) over a) S3VT SP-Val semi-arid mediterranean and b) SP-Ala cultivated areas. (For interpretation of the references to colour in this figure legend, the reader is referred to the web version of this article.)

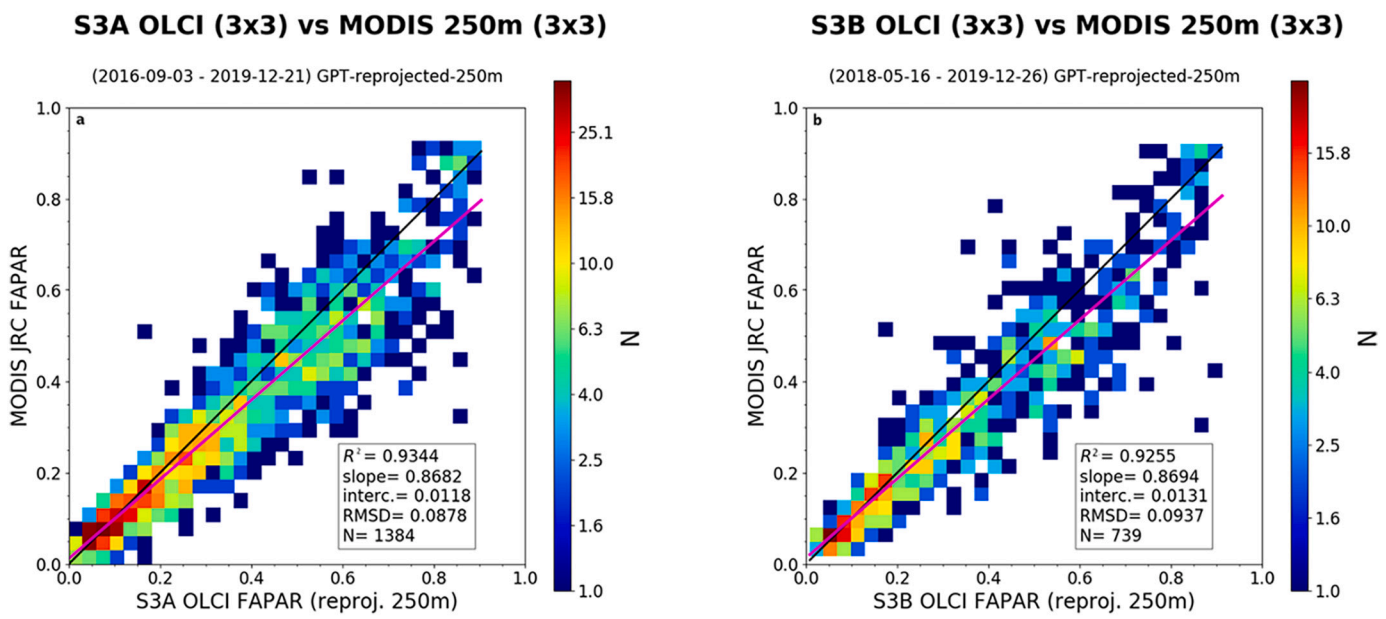

Fig. 10. Comparisons between daily S3A-OLCI (a) and S3B-OLCI (b) against JRC FAPAR MODIS over all the S3VT sites.

(Fig. 8a). We have the same outcome over IT-Isp except for 2018 at the start of the growing season (Fig. 8b). Conversely, over IT-Sro, the 2018 values are highest amongst all the years and the climatology (Fig. 8c).

The fact that climatology values are lower than OLCI ones may be because the MERIS third-reprocessing was missing additional land products Quality and Science Flags (QSF) such as CLOUD_AMBIGUOUS and CLOUD_MARGIN. Hence, unflagged cloud/cloud shadow contaminations may decrease the MERIS derived climatology values of FAPAR when compared to OLCI.

The two last profiles are over the semi-arid Mediterranean site, SP-Val, and cultivated areas SP-Ala are displayed in Fig. 9a and Fig. 9b, respectively. Both seasonalities and FAPAR values agree well but with inter-annual variations that may arise from different climatic conditions.

3.3. JRC-FAPAR using MODIS and Sentinel-2 MSI data

The initial comparison was made against JRC-FAPAR MODIS products at 250 m over all the S3VT sites over several years. Average values were taken over a 3×3 pixels grid using only valid pixels, i.e. 100% coverage, to avoid any cloud or cloud-shadow contaminations and to decrease the impact of sensors' geo-location. Fig. 10 shows the results of comparisons against a) MODIS for S3A and b) S3B. As the S3B data availability is less than the S3A one, the number of match-up points drops from 1384 to 739. The day lag between MODIS and OLCI dates is ± 1 day. The results show that the S3A (S3B) OLCI products agree with MODIS with an RMSD of 0.0878 (0.0937). This benchmark was done after remapping the OLCI products at 250 m. Note that the JRC MODIS FAPAR algorithm at 250 m used the blue band which is originally at 500 m (see Gobron et al., 2006a): these may include geographical mismatches and then explain a strong deviation in the regression line.

The second comparison was done using S2 MSI data for which JRC FAPAR was computed at 60 m spatial resolution over the S3VT sites. Spatial averages from S2 at 60 m to 300 m (900 m) were calculated using only fully valid pixels to remove cloud or cloud-shadow contaminations. Fig. 11 displays the scatter-plots between S3A (a-b) and S3B (c-d) against S2A/B at 300 m (a-c) and 900 m (b-d), respectively. The maximum time lag between S2 and S3 dates is ± 4 days. The results show a better agreement when using 900 m spatial resolution as geolocation issues and contamination of cloud/cloud shadow are reduced. RMSD values are at about 0.062 (0.069) for S3A (S3B) at 900 m and 0.088 (0.095) at 300 m, respectively. The slight bias is also explained by the non-linearity of radiative transfer theory: it makes a difference whether we aggregate FAPAR products generated at the native resolution (e.g. 60 m to 300 m) or compute the FAPAR on the aggregated spectral bands (Kaminski et al., 2017). Times of acquisition of both instruments are not the same as the S3 orbit is a near-polar, sun-synchronous orbit with a descending node equatorial crossing at 10:00 Mean Local Solar time (MLST) whereas the MLST of S2 at the descending node is 10:30.

3.4. Ground-based measurements

In order to check the consistency and seasonality of OLCI FAPAR, we first plot time series of various in-situ ground-based data that were not up-scaled, per se. Issues concern the availability of uncertainties of such data and their spatial representation, as well as the geo-location differences between them and OLCI observations. In addition, the so-called 'green' FAPAR calculated using Eq. 1 with the assumption of a linear correlation between LAI and FAPAR inevitably introduces some errors for the US-Ne sites. Nevertheless, these ground-based measurements represent well the seasonality during the growing season as shown in Fig. 12. Satellite and ground-based FAPAR estimations over the three USA sites compare very well with each other during the growing period. The OLCI products show systematically lower values (about 0.1) than the ground-based estimations during the summer season. The measurements derived from DHP were also plotted over the New Forest site, UK-NFo (Fig. 13a): only few in-situ measurements were available for 2016 (Brown et al., 2019). They were adjusted using 3D-RT simulations correction factors as explained in Section 2. The S3 FAPAR vary from year to year. Up to the senescence phase, we found the same range of values by both measurement types whereas the ones in October show a large difference up to 0.2.

Over the AMMA-CATCH sites in Mali, we see that the phenology from in-situ and EO products was well represent over the four types of vegetation. However, the expected negative bias over the Acacia forest can be seen during the winter season (Fig. 13e). Over the Direct 2.0 sites, we found a very good agreement with RMSD of 0.07 with a bias of 0.05 (not shown).

The results using ground-based measurements from the Copernicus GBOV service are shown in Fig. 14. Each panel shows the scatter-plot between a) S3A OLCI and b) S3B OLCI against the FIPAR value of the GBOV LP4 products (Version 2.1). RMSD was computed for the different types of vegetation. OLCI products and the ground-based values agreed

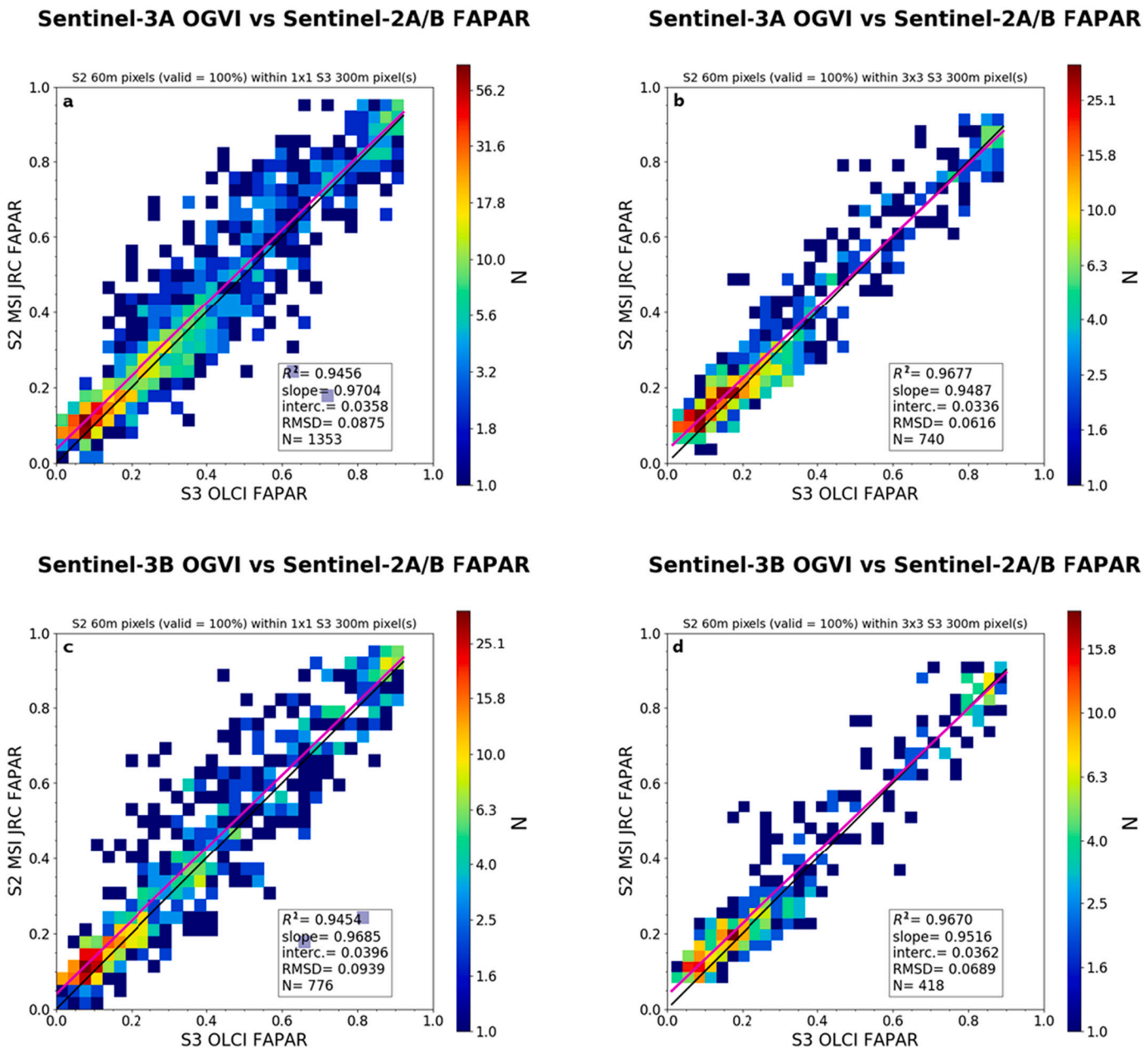

Fig. 11. Comparisons between daily FAPAR from S3A (a and b) and S3B (c and d) OLCI against JRC FAPAR MSI S2A/S2B using at 300 m (a and c) and 900 m (b and d) over all S3VT sites.

generally within ±0.10, which is within the expected bias when using FIPAR as a proxy of FAPAR (Gobron et al., 2006b). Over the mixed forest (dark blue symbols), OLCI FAPAR values are smaller than the ground-based ones.

To analyse better the results in term of uncertainty closure assessment, we plot the variance between EO data and in-situ measurements against the total uncertainties, i.e. the square root of the sum of squares of each uncertainty, together with their frequencies as proposed by Immler et al. (2010) over three types of land cover for each sensor Fig. 15. They indicate that the variances between EO and ground-based products and the total uncertainties are within ±0.1 over forest sites. 35% of the points have a total uncertainty value of 0.05 together with a very small variance. The total uncertainties show greater fluctuations for cropland and grassland sites with a maximum of 0.4 respectively, but with smaller variances.

3.5. 3D-RT modelling over the QA4ECV sites

Simulations of various types of FAPAR ground-based measurements were compared to FAPAR computed with two years of daily OLCI TOA simulations that coupled Raytran and 6S models. The reference FAPAR values correspond to the 2-flux, 4-flux estimates and actual foliage absorption, the latter of which can only be computed through model simulations (as the absorption from flux measurements can only be associated to the whole canopy, including leaves, trunks and stem elements). Fig. 16 shows the scatter-plots between OLCI FAPAR and 3D-RT reference values for each virtual site and in-situ definition. It demonstrates that the evolution of validation results depends on the in-situ measurement definition together with the type of vegetation cover. In general, the results are much better when the foliage absorption is used, as was expected. However, the OLCI FAPAR values were close to the

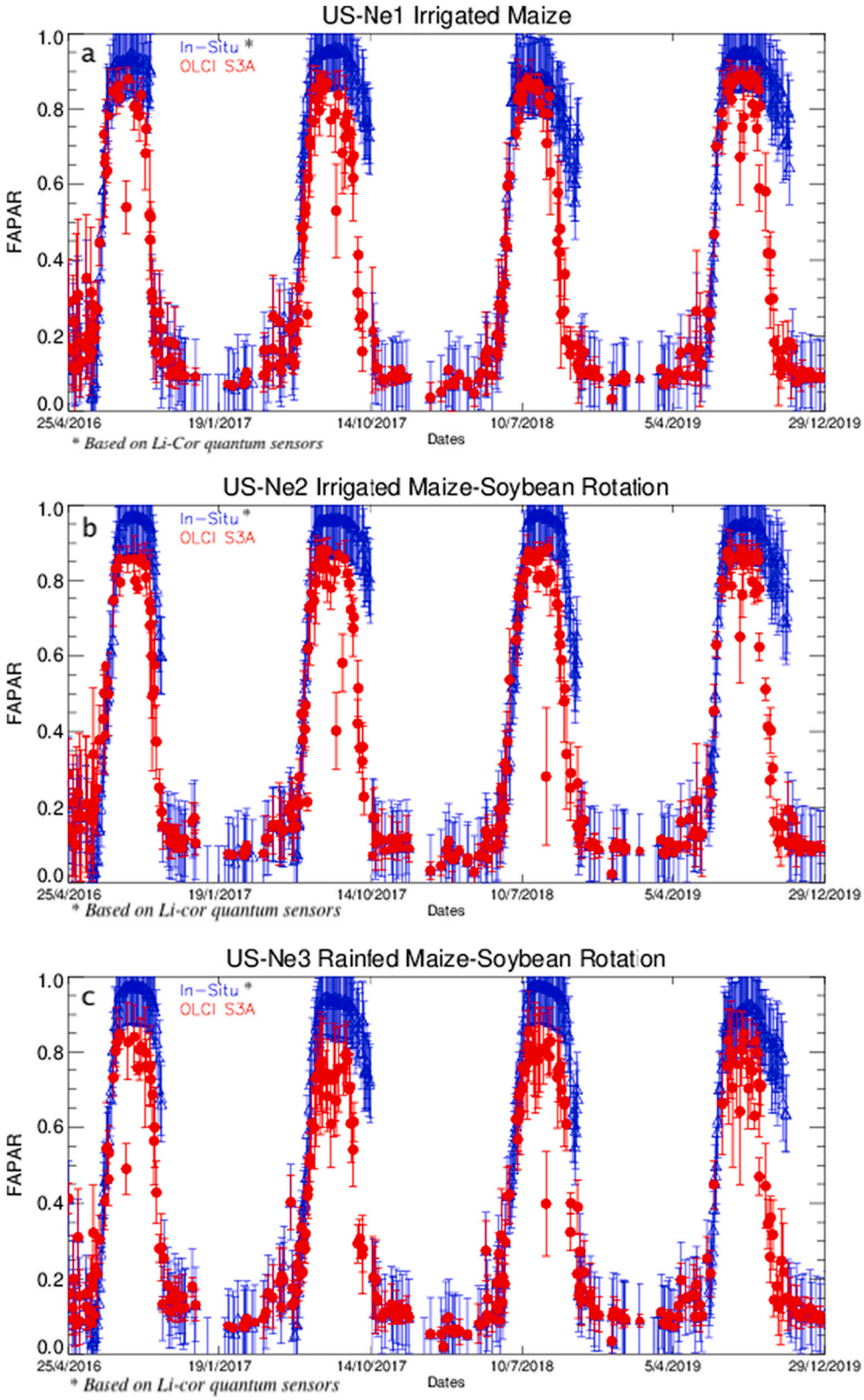

Fig. 12. Time series of daily OLCI S3A and in-situ data, based on Li-cor quantum sensors, over a) US-Ne1, b) US-Ne2 and c) US-Ne3 sites.

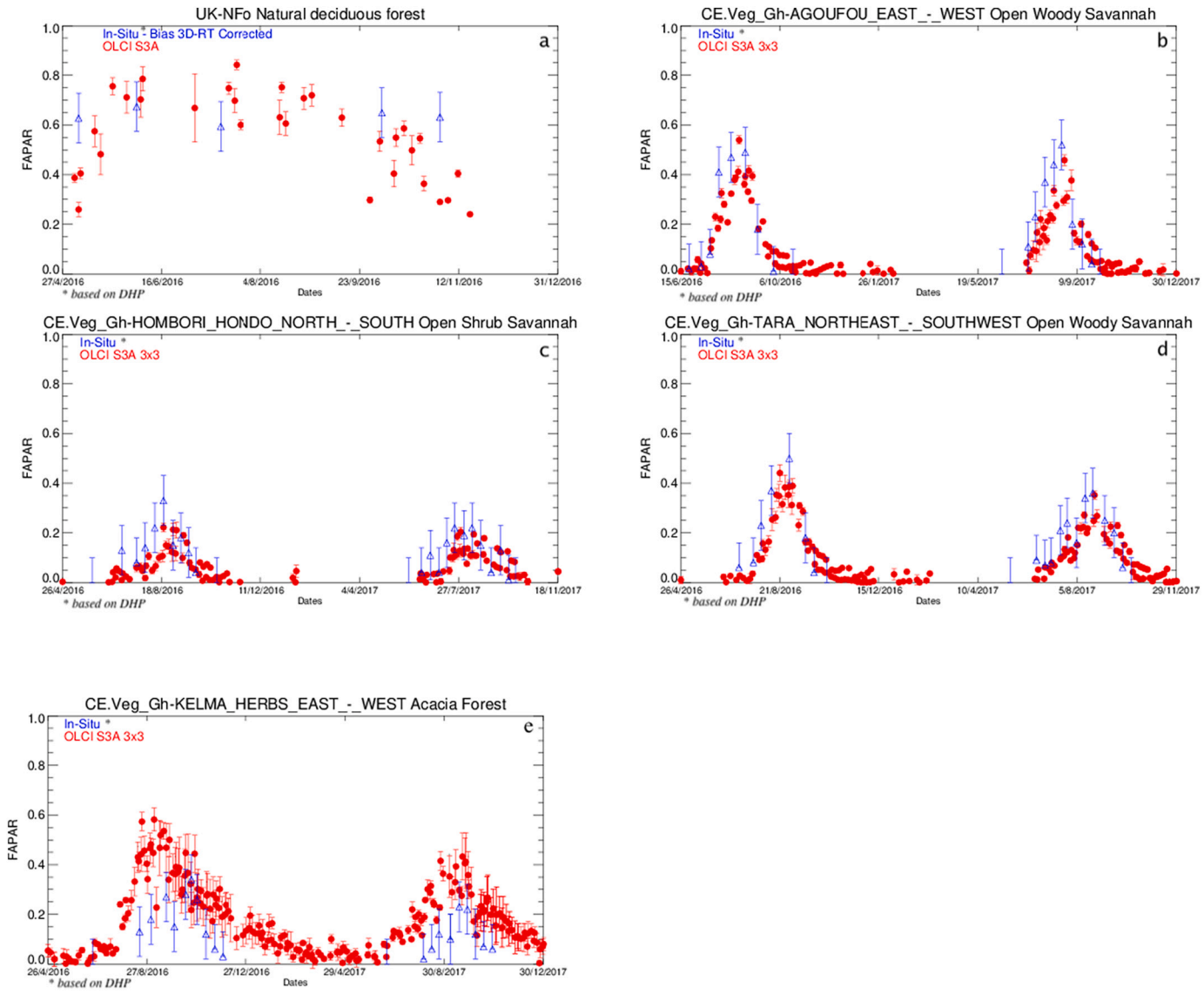

Fig. 13. Time series of daily OLCI S3A and in-situ data, based on DHP, over a) UK-NFo b-e) AMMA-CATCH sites.

fluxes measurements for the Nghotto forest and Skukuza savannah and disagreed when the foliage absorption was taken as reference. In the first case, the foliage absorption was smaller than with the 2- and 4-flux methods because of the strong contribution of woody elements. In the second case, the value was much larger and deviated from the OLCI results, mainly because of the understory (grass) contribution to absorption of the Savannah scene (Disney et al., 2011), which was not considered in 2- or 4-flux modelling. Over the LOPE tropical forest site, the biases were always higher than 0.25 in all reference cases. This may be due to spectral values associated to the scene. Fig. 17 illustrates the histogram of variance between references and OLCI results as function of their associated uncertainties. We can see that except for the small values the agreement in term of variance is better for the foliage absorption.

4. Discussion

4.1. Impact of spectral response

Recently, Lamquin et al. (2020a) indicate that even though OLCI-A and OLCI-B have the same design characteristics, they do not have the identical spectral characterisation nor radiometric and geometric calibrations. These small dissimilarities impact the Level 1 data and therefore Level 2 as well. Lamquin et al. (2020b) showed the impacts of spectral response at the level of each detector over Amazonia and Europe and found that calibration correction reduces the relative differences to 0.7%. In this paper, the small spectral response difference for S3A and S3B impact the green FAPAR values with a bias at about 0.003 in monthly products during the tandem period at the global scale. It means that S3A FAPAR is slightly higher than S3B, which is within the range of the uncertainties. Nevertheless, the foreseen correction of L1 will positively impact the FAPAR consistency between the two platforms. When we compare S3A/S3B against JRC products using MODIS or S2 data, we consider the differences of sensor spectral responses through the retrieval algorithm as each spectral response were used in the radiative transfer simulations to optimize both rectified channels and FAPAR equations.

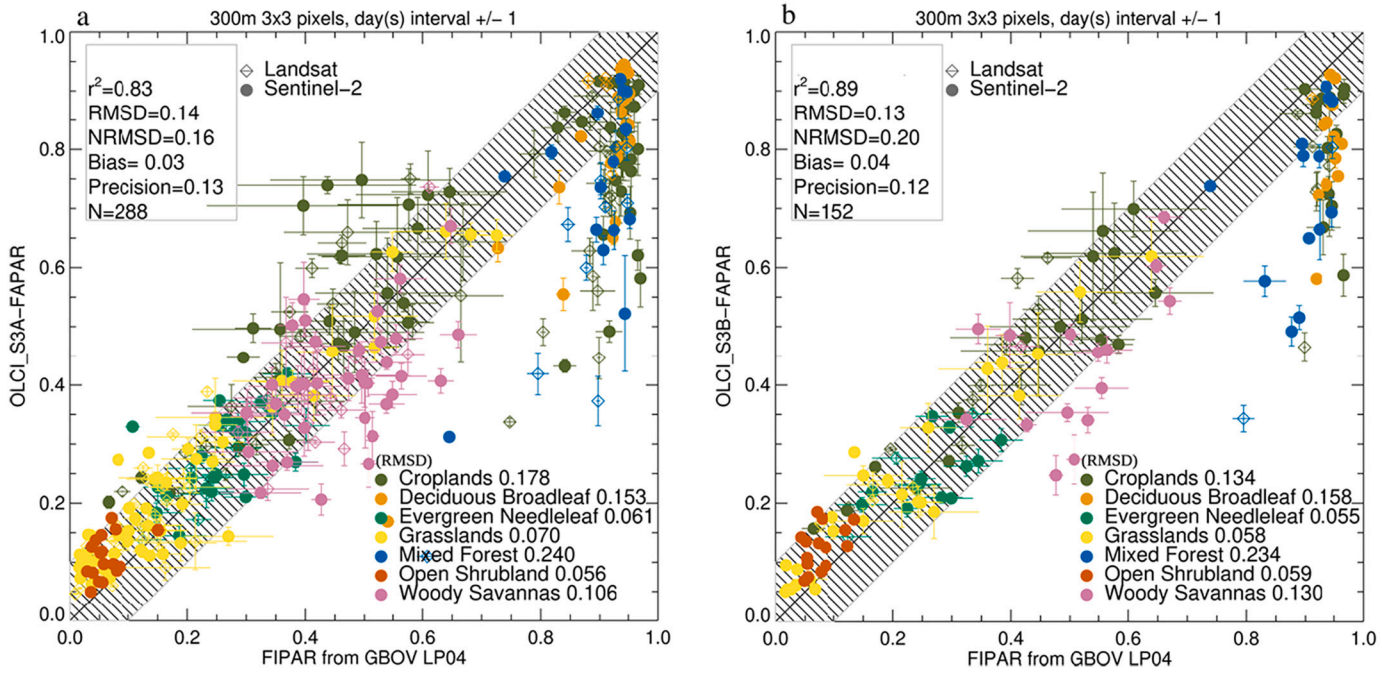

Fig. 14. Comparisons between daily green instantaneous FAPAR from a) S3A OLCI and b) S3B OLCI against FIPAR GBOV LP4 products. (For interpretation of the references to colour in this figure legend, the reader is referred to the web version of this article.)

4.2. *Impact of time of acquisition and spatial scale*

The JRC FAPAR is defined to be the instantaneous value at the time of acquisition. As there is around 30 min between OLCI and MODIS, this small difference in illumination geometries condition has almost no impact between the products. Li and Fang (2015) showed the instantaneous values of FAPAR as function of sun zenith angle for several LAI using radiative transfer model. The main sources of potential discrepancies are indeed the difference in their viewing geometries and their spatial resolution as OLCI and MODIS sensors do not have the same technical characteristics. MODIS is a scanner (250 m at nadir view) whereas OLCI (300 m) is a push-broom imaging spectrometer with five cameras: therefore, original pixels do not have the spatial resolution nor are they geo-located. To benchmark EO products, remapping them over a geographical grid is mandatory and therefore includes some geo-spatial uncertainties, specially for vegetated areas that are not homogenous. Any remapping step should be added for deriving additional uncertainties when comparing EO products as discussed on Loew et al. (2017).

4.3. *'Mixture' of ground-based measurements*

Unfortunately, ground-measurements providing the exact same quantity as the Earth Observation products, i.e. green foliage absorption at time of sensor of acquisition, were not available. In this paper, we thus relied only on a limited number of proxy data sets that were available mainly over the North American continent using GBOV data (Version 2.1). We indeed used various sources of in-situ measurements over different types of vegetation coming from different projects. These ground-based measurements were mainly derived from DHP techniques, using different sampling or/and up-scaling protocols and few of them came from hourly Li-Cor quantum measurements. None of them represents the actual FAPAR OLCI definition, but as already shown in Gobron et al. (2008), these data are valuable as proxy to assess its quality within a certain range of uncertainties, i.e. $+/-$ 0.1. Depending on the type of land cover, these ground-based measurements may serve a good proxy for seasonality of vegetated activities. The difference between the total absorbed value and that of the foliage simulated by the 3D-RT model for the Järvselja-2 site was used for the New Forest canopy, only. As pointed out in Niro et al. (2021), radiative transfer modelling should play a future and very important role in correcting ground measurements. This would require additional measurements so that all the spectral and structural variables used in a 3D-RT model are known and would also allow realizing the uncertainty budget for the validation data. Even so there are now few vegetation Fiducial Reference Measurements (FRM) (Brown et al., 2021a, 2021b), they still do not supply this required information to infer the foliage values.

The main outliers were due to the limitations of using DHP methodology in forest environments during and after the senescence period and winter. Using the total intercepted radiation to infer FIPAR with DHP instead of the (green) foliage absorption induced a strong difference as shown by the 3D-RT simulations.

5. Conclusions

The performance of both S3A and S3B OLCI terrestrial products was assessed using various methods, including comparison with MODIS and S2 MSI data using the same retrieval algorithm, various type of ground-based measurements and 3D-RT modelling virtual simulations. We found that during the tandem phase period, S3A and S3B provided the almost identical values of FAPAR at global scale with RMSD <0.02 and $R^2 = 0.99$. This means that with these twin Copernicus S3 OLCI instruments, the number of observations provides users with increased geographical and temporal global coverage. Using 'match-up' daily products from JRC FAPAR MODIS and JRC FAPAR S2 MSI, we showed that the agreement achieved the expected goal of R^2 greater than 0.9 and RMSD less than 0.1 over the S3VT sites. The fact that daily S2 MSI and daily S3 OLCI can provide the same values at different scales also opens the range of Copernicus applications such as agriculture management and local to regional climate adaptation studies.

By filtering the good quality values in both space and up-scaled ground-measurements (GBOV LP4), we found that 65% of OLCI products at 300 m spatial resolution were within ± 0.1 of uncertainties that could be expected when comparing intercepted and absorbed components (Gobron et al., 2006b). Using the AMMA-CATCH measurements, we checked the seasonality over additional locations covering other type

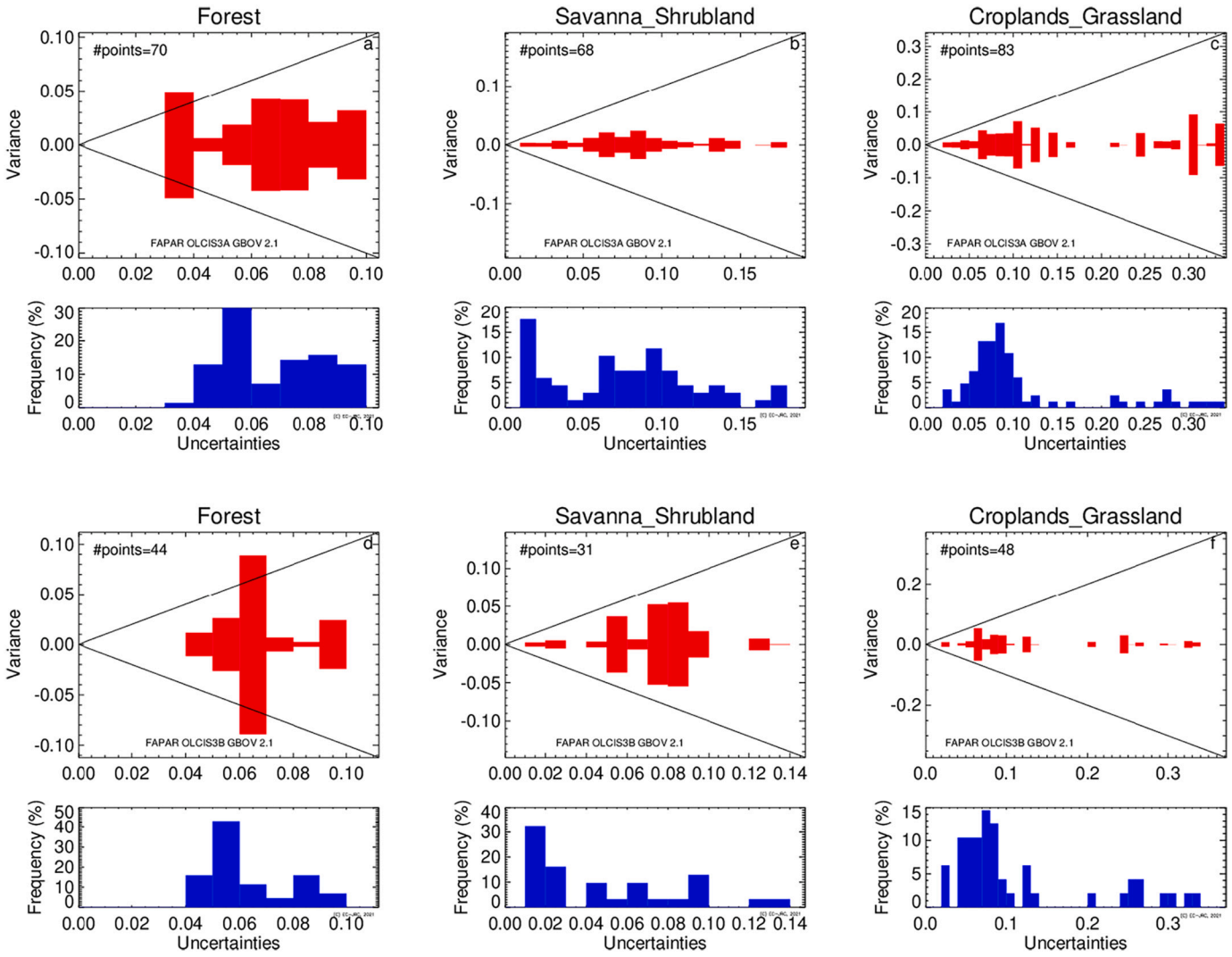

Fig. 15. Variance against total uncertainties (with frequency) for the daily green instantaneous FAPAR from S3A (top panels) and S3B (bottom panels) OLCI for a-d) Forest b-e) Savanna and Shrubland and c-f) Cropland and Grassland. (For interpretation of the references to colour in this figure legend, the reader is referred to the web version of this article.)

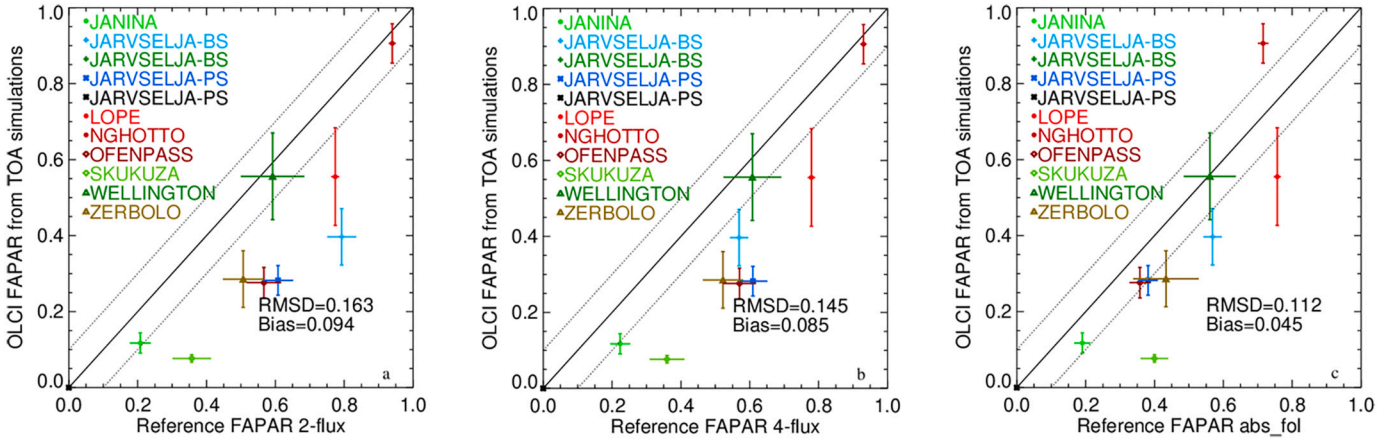

Fig. 16. FAPAR using OLCI simulations data against a) 2-flux, b) 4-flux and c) actual foliage absorption (abs_fol) as reference values.

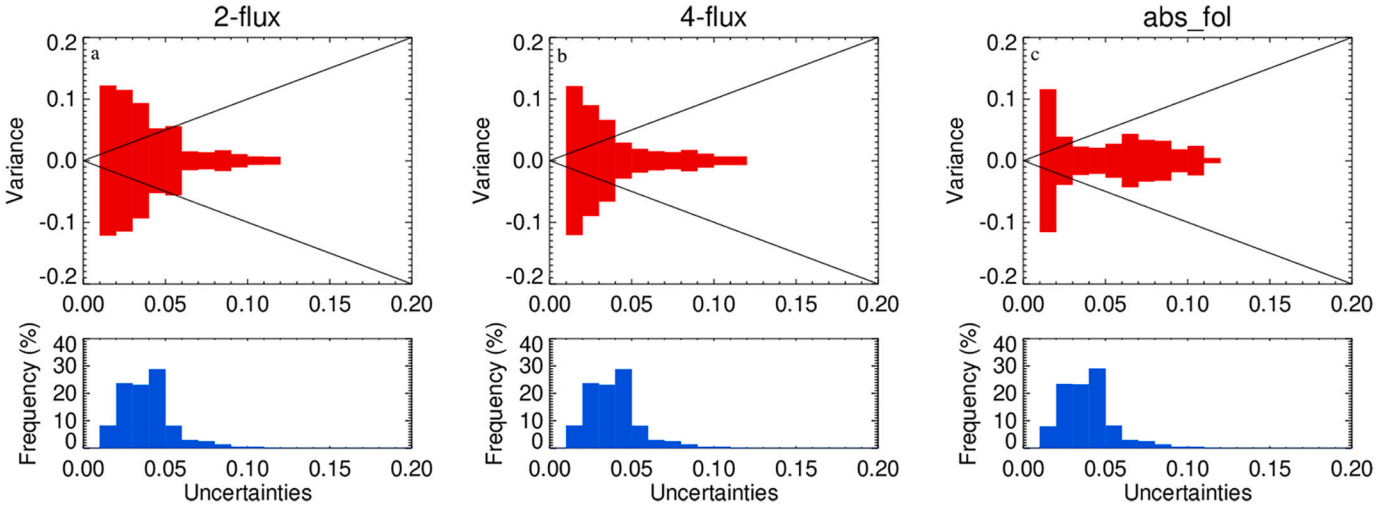

Fig. 17. Variance versus the uncertainty of JRC FAPAR from OLCI simulations over 2 years of simulations using a) 2-flux, b) 4-flux and c) actual foliage absorption (abs_fol) as reference values.

of land cover. We found a good agreement over low vegetation sites and same phenology over Acacia Forest.

The results from the 3D-RT modelling demonstrated that bias should decrease when using the foliage absorption as the reference. As foliage absorption is very difficult to measure at ground-level, there is a need to correct in-situ data for biases, using modelling studies, in future validation frameworks.

The next generation of GBOV measurements will provide such ground-based data using Wireless Sensor Networks (WSNs) as performed in Putzenlechner et al., (2019). Finally, supplementary work should focus on validating the uncertainties of OLCI FAPAR that will be available, at pixel level, in the near future.

Credits authors

N.G. conceived and designed the validation study. O.M., F·C, M.M. and M.R. contributed to the data processing. J.A and C.L. make the 3D-RT DHP and OLCI spectral reflectance simulations. L.B. and J.D. performed the New Forest in-situ campaign and provided the GBOV LPs datasets. NG wrote the manuscript. All co-authors reviewed the manuscript.

Declaration of Competing Interest

The authors declare that they have no known competing financial interests or personal relationships that could have appeared to influence the work reported in this paper.

Acknowledgments

This study has been undertaken using LP4 data from GBOV "Ground Based Observation for Validation" (https://land.copernicus.eu/global/gbov) established by the European Commission Joint Research Centre FWC932059, part of the Global Component of the European Union's Copernicus Land Monitoring Service. GBOV products are developed and managed by ACRI-ST with the support from University College London, University of Leicester, University of Southampton, University of Valencia and Informus GmbH. The support provided by DG DEFIS, i.e. the European Commission Directorate-General for Defence Industry and Space, and Copernicus Programme is gratefully acknowledged. The AMMA-CATCH regional observing system (http://www.amma-catch.org) was set up thanks to incentive funding from the French Ministry of Research that allowed pooling together of various pre-existing small scale observation setups. The continuity and long term durability of the measurements are made possible by the undisrupted IRD funding since 1990 and by continuous CNRS-INSU funding since 2005.

The first author acknowledges Anatoly Gitelson and Andrew E. Suyker for their past and continuous support with the Nebraska data, and Ludovic Bourg (ACRI/MPC) for the OLCI data access.

References

Adams, J., Gobron, N., Mio, C., 2016. A study of land surface albedo conversion formulae using 3D canopy radiative transfer modeling. IEEE Trans. Geosci. Remote Sens. 13, 1039–1043. https://doi.org/10.1109/LGRS.2016.2535160.

Brown, L.A., Ogutu, B.O., Dash, J., 2019. Estimating forest leaf area index and canopy chlorophyll content with Sentinel-2: an evaluation of two hybrid retrieval algorithms. Remote Sens. 2019 11 (15), 1–17 [1752]. https://doi.org/10.3390/rs11151752.

Brown, L.A., Meier, C., Morris, H., Pastor-Guzman, J., Bai, G., Lerebourg, C., Gobron, N., Lanconelli, C., Clerici, N., Dash, J., 2020. Evaluation of global leaf area index and fraction of absorbed photosynthetically active radiation products over North America using Copernicus ground based observations for validation data. Remote Sens. Environ. 247 (111935), 2020. https://doi.org/10.1016/j.rse.2020.111935.

Brown, L.A., Fernandes, R., Djamai, N., Meier, C., Gobron, N., Morris, H., Canisius, F., Bai, G., Lerebourg, C., Lanconelli, C., Clerici, M., Dash, J., 2021a. Validation of baseline and modified Sentinel-2 level 2 prototype processor leaf area index retrievals over the United States. ISPRS J. Photogramm. Remote Sens. 175, 71–87. https://doi.org/10.1016/j.isprsjprs.2021.02.020.

Brown, L.A., Camacho, F., García-Santos, V., Origo, N., Fuster, B., Morris, H., Pastor-Guzman, J., Sánchez-Zapero, J., Morrone, R., Ryder, J., Nightingale, J., Boccia, V., Dash, J., 2021b. Fiducial reference measurements for vegetation bio-geophysical variables: an end-to-end uncertainty evaluation framework. Remote Sens. 13 (16), 3194. https://doi.org/10.3390/rs13163194.

Calders, K., Origo, N., Disney, M., Nightingale, J., Woodgate, W., Armston, J., Lewis, P., 2018. Variability and bias in active and passive ground-based measurements of effective plant, wood and leaf area index. Agric. For. Meteorol. 252, 231–240. https://doi.org/10.1016/j.agrformet.2018.01.029.

Chernetskiy, M., Gomez-Dans, J., Gobron, N., Morgan, O., Lewis, P., Truckenbrodt, S., Schmullius, C., 2017. Estimation of FAPAR over croplands using MISR data and the earth observation land data assimilation system (EO-LDAS). Remote Sens. 9, 656. https://doi.org/10.3390/rs9070656.

Disney, M.I., Lewis, P., Gomez-Dans, J., Roy, D., Wooster, M.J., Lajas, D., 2011. 3D radiative transfer modelling of fire impacts on a two-layer savanna system. Remote Sens. Environ. 115 (8), 1866–1881. https://doi.org/10.1016/j.rse.2011.03.010.

Donlon, C., Berruti, B., Buongiorno, A., Ferreira, M.H., Féménias, P., Frerick, J., Goryl, P., Klein, U., Laur, H., Mavrocordatos, C., Nieke, J., Rebhan, H., Seitz, B., Stroede, J., Sciarra, R., 2012. The global monitoring for environment and security (GMES) Sentinel-3 mission. Remote Sens. Environ. 120, 37–57. The Sentinel Missions - New Opportunities for Science. https://doi.org/10.1016/j.rse.2011.07.024.

Drusch, M., Bello, U.D., Carlier, S., Colin, O., Fernandez, V., Gascon, F., Hoersch, B., Isola, C., Laberinti, P., Martimort, P., Meygret, A., Spoto, F., Sy, O., Marchese, F., Bargellini, P., 2012. Sentinel-2: ESA's optical high-resolution mission for GMES operational services. Remote Sens. Environ. 120, 25–36. https://doi.org/10.1016/j.rse.2011.11.026.

Galle, S., et al., 2018. AMMA-CATCH, a critical zone observatory in West Africa monitoring a region in transition. Vadose Zone J. 17, 180062 https://doi.org/10.2136/vzj2018.03.0062.

Garrigues, S., Lacaze, R., Baret, F., Morisette, J.T., Weiss, M., Nickeson, J.E., Fernandes, R., Plummer, S., Shabanov, N.V., Myneni, R.B., Knyazikhin, Y., Yang, W., 2008. Validation and intercomparison of global leaf area index products derived from remote sensing data. J. Geophys. Res. 113, G02028. https://doi.org/10.1029/2007JG000635.

GCOS, 2016. Summary Report of the eleventh session of the WMO-IOC-UNEP-ICSU (WMO/TD-No.1189). Report Melbourne, Australia, April 7-10 GCOS-87. World Meteorological Organization, 2016.

Gitelson, A.A., Viña, A., Arkebauer, T.J., Rundquist, D.C., Keydan, G., Leavitt, B., 2003. Remote estimation of leaf area index and green leaf biomass in maize canopies. Geophys. Res. Lett. 30 (5), 1248. https://doi.org/10.1029/2002GL016450.

Gitelson, A.A., Peng, Y., Huemmrich, K.F., 2014. Relationship between fraction of radiation absorbed by photosynthesizing maize and soybean canopies and NDVI from remotely sensed data taken at close range and from MODIS 250 m resolution data. Remote Sens. Environ. 147, 108–120. https://doi.org/10.1016/j.rse.2014.02.014.

Gobron, N., 2011. Ocean and Land Colour Instrument (OLCI) FAPAR and Rectified Channels over Terrestrial Surfaces Algorithm Theoretical Basis Document. Technical report. Institute for Environment and Sustainability.

Gobron, N., Pinty, B., Verstraete, M.M., Govaerts, Y., 1997. A semi-discrete model for the scattering of light by vegetation. J. Geophys. Res. 102, 9431–9446. https://doi.org/10.1029/96JD04013.

Gobron, N., Pinty, B., Mélin, F., Taberner, M., Verstraete, M.M., 2002. Sea Wide Field-of-View Sensor (SeaWiFS) - An Optimized FAPAR Algorithm - Theoretical Basis Document. EUR Report No. 20148 EN. Institute for Environment and Sustainability.

Gobron, N., Aussédat, O., Pinty, B., Taberner, M., Verstraete, M.M., 2004. Medium Resolution Imaging Spectrometer (MERIS) - Level 2 Land Surface Products - Algorithm Theoretical Basis Document-Revision 3.0. EUR Report No. 21387 EN. Institute for Environment and Sustainability.

Gobron, N., Aussédat, O., Pinty, B., 2006a. MODerate Resolution Imaging Spectroradiometer (MODIS) - JRC-FAPAR at 250m Algorithm Theoretical Basis Document. EUR Report 22279 EN. European Commission - DG Joint Research Centre, Institute for Environment and Sustainability.

Gobron, N., Pinty, B., Aussédat, O., Chen, J.M., Cohen, W.B., Fensholt, R., Gond, V., Huemmrich, K.F., Lavergne, T., Mélin, F., Privette, J.L., Sandholt, I., Taberner, M., Turner, D.P., Verstraete, M.M., Widlowski, J.L., 2006b. Evaluation of FAPAR products for different canopy radiation transfer regimes: methodology and results using JRC products derived from SeaWiFS against ground-based estimations. J. Geophys. Res.-Atmos. 111 https://doi.org/10.1029/2005JD006511.

Gobron, N., Pinty, B., Aussédat, O., Taberner, M., Faber, O., Mélin, F., Lavergne, T., Robustelli, M., Snoeij, P., 2008. Uncertainty estimates for the FAPAR operational products derived from MERIS - impact of top-of-atmosphere radiance uncertainties and validation with field data. Remote Sens. Environ. 112, 1871–1883. https://doi.org/10.1016/j.rse.2007.09.011.

Gobron, N., Dash, J., Lopez Baeza, E., Cescatti, A., Gitelson, A., Gruening, C., Schmullius, C., Widlowski, J.L., 2013. SENTINEL-3 Ocean Land Color Imager (OLCI): Land products and validation. In: Ouwehand, L. (Ed.), Proceedings of the 2013 ESA Living Planet Symposium, 9-13 September 2013, Edinburgh, UK, Issue SP-722, ISBN 978–92–9221-286-5, 2013.

Gobron, N., Marioni, M., Robustelli, M., Vermote, E., 2019. Can we use the QA4ECV black-sky fraction of absorbed photosynthetically active radiation (FAPAR) using AVHRR surface reflectance to assess terrestrial global change? Remote Sens. 11 (24) https://doi.org/10.3390/rs11243055.

Govaerts, Y., Verstraete, M.M., 1998. Raytran: a Monte Carlo ray tracing model to compute light scattering in three-dimensional heterogeneous media. IEEE Trans. Geosci. Remote Sens. 36, 493–505.

Gruening, C., Goded, I., Cescatti, A., Fachinetti, D., Fumagalli, I., Duerr, M., 2012. ABC-IS Forest Flux Station–Report on Instrumentation, Operational Testing and First Months of Measurements. Publications Office of the European Union, Luxembourg. https://doi.org/10.2788/7774, 19 pp. – 21.0 x 29.7 cm EUR – Scientific and Technical Research series – ISSN 1831-9424 - ISBN 978-92-79-28104-4.

Immler, F.J., Dykema, J., Gardiner, T., Whiteman, D.N., Thorne, P.W., Vömel, H., 2010. Reference quality upper-air measurements: guidance for developing GRUAN data products. Atmos. Measure Tech. 3, 1217–1231. https://doi.org/10.5194/amt-3-1217-2010.

Kaminski, T., Pinty, B., Voßbeck, M., Lopatka, M., Gobron, N., Robustelli, M., 2017. Consistent EO land surface products including uncertainty estimates. Biogeosci. Discuss. 2017 https://doi.org/10.5194/bg-2016-310.

Kotchenova, S., Vermote, E., Matarrese, R., Klemm Jr., F., 2006. Validation of a vector version of the 6S radiative transfer code for atmospheric correction of satellite data. Part I: path radiance. Appl. Opt. 45, 6726–6774. https://doi.org/10.1364/AO.45.006762.

Lamquin, N., Clerc, S., Bourg, L., Donlon, C., 2020a. OLCI A/B tandem phase analysis, part 1: level 1 homogenisation and harmonisation. Remote Sens. (12), 1804. https://doi.org/10.3390/rs12111804, 2020.

Lamquin, N., Déru, A., Clerc, S., Bourg, L., Donlon, C., 2020b. OLCI A/B tandem phase analysis, part 2: benefits of sensors harmonisation for level 2 products. Remote Sens. 12, 2702. https://doi.org/10.3390/rs12172702, 2020.

Lanconelli, C., Gobron, N., Adams, J., Danne, O., Blessing, S., Robustelli, M., Kharbouche, S., Muller, J.P., 2018. Report on the Quality Assessment of Land ECV retrieval algorithms. Scientific and Technical Report JRC109764. Joint Research Centre.

Levy, R., Hsu, C., et., al., 2015. MODIS Atmosphere L2 Aerosol Product. NASA MODIS Adaptive Processing System. Goddard Space Flight Center, USA. https://doi.org/10.5067/MODIS/MOD04_L2.006 (Terra) and doi: https://doi.org/10.5067/MODIS/MYD04_L2.006 (Aqua).

Li, W., Fang, H., 2015. Estimation of direct, diffuse, and total FPARs from Landsat surface reflectance data and ground-based estimates over six FLUXNET sites. J. Geophys. Res. Biogeosci. 120, 96–112. https://doi.org/10.1002/2014JG002754.

Loew, A., Bell, W., Brocca, L., Bulgin, C.E., Burdanowitz, J., Calbet, X., Donner, R.V., Ghent, D., Gruber, A., Kaminski, T., Kinzel, J., Klepp, C., Lambert, J.C., Schaepman-Strub, G., Schröder, M., Verhoelst, T., 2017. Validation practices for satellite-based earth observation data across communities. Rev. Geophys. 55, 779–817. https://doi.org/10.1002/2017RG000562.

Lopez-Baeza, E., Antolin, C., Belda, F., Carbo, E., Coll, A., et al., 2013. SMOS land validation activities at the Valencia Anchor Station. In: XV Congreso de la Asociación Española deTeledetección INTA, Oct 2013, Torrejón de Ardoz (Madrid), Spain hal-01190018.

Mougin, E., Demarez, V., Diawara, M., Hiernaux, P., Soumaguel, N., Berg, A., 2014. Estimation of LAI, fAPAR and fCover of Sahel rangelands (Gourma, Mali). Agric. For. Meteorol. 198–199, 155–167. ISSN 0168–1923. https://doi.org/10.1016/j.agrformet.2014.08.006.

Niro, F., Goryl, P., Dransfeld, S., Boccia, V., Gascon, F., Adams, J., Themann, B., Scifoni, S., Doxani, G., 2021. European Space Agency (ESA) calibration/validation strategy for optical land-imaging satellites and pathway towards interoperability. Remote Sens. 13 (15), 3003. https://doi.org/10.3390/rs13153003.

Putzenlechner, B., Castro, S., Kiese, R., Ludwig, R., Marzahn, P., Sharp, I., Sanchez-Azofeifa, A., 2019. Validation of Sentinel-2 fAPAR products using ground observations across three forest ecosystems. Remote Sens. Environ. 232, 111310. ISSN 0034–4257. https://doi.org/10.1016/j.rse.2019.111310.

Rahman, H., Pinty, B., Verstraete, M.M., 1993. Coupled surface-atmosphere reflectance (CSAR) model. 2. Semi-empirical surface model usable with NOAA advanced very high resolution radiometer data. J. Geophys. Res. 98, 20791–20801. https://doi.org/10.1029/93JD02072.

Suyker, A., 2021. AmeriFlux US-Ne1 Mead - Irrigated Continuous Maize Site, Ver. 10-5, AmeriFlux AMP (Dataset). https://doi.org/10.17190/AMF/1246084.

Truckenbrodt, S.C., Baade, J., 2018. Agricultural Gebesee test site (central Germany): extent and location of acreages investigated in 2013 and 2014; PANGAEA, 2017. In supplement to: Truckenbrodt, S. C and Schmullius, C (2018): Seasonal evolution of soil and plant parameters on the agricultural Gebesee test site: a database for the set-up and validation of EO-LDAS and satellite-aided retrieval models. Earth Syst. Sci. Data 10 (1), 525–548 doi:https://doi.org/10.5194/essd-10-525-2018.

Vermote, E., Tanré, D., Deuzé, J.L., Herman, M., Morcrette, J.J., 1997. Second simulation of the satellite signal in the solar spectrum: an overview. IEEE Trans. Geosci. Remote Sens. 35-3, 675–686. https://doi.org/10.1109/36.581987.

Viña, A., Gitelson, A.A., 2005. New developments in the remote estimation of the fraction of absorbed photosynthetically active radiation in crops. Geophys. Res. Lett. 32 https://doi.org/10.1029/2005GL023647.

Vuolo, F., Dash, J., Curran, P.J., Lajas, D., Kwiatkowska, E., 2012. Methodologies and uncertainties in the use of the terrestrial chlorophyll index for the Sentinel-3 mission. Remote Sens. 4, 1112–1133.

Weiss, M., Baret, F., 2014. CAN-EYE UserManual. https://www6.paca.inra.fr/can-eye.

Weiss, M., Baret, F., 2016. S2ToolBox Level 2 Products: LAI, FAPAR, FCOVER ed. Institut National de la Recherche Agronomique, Avignon, France. https://step.esa.int/docs/extra/ATBD_S2ToolBox_L2B_V1.1.pdf.

Widlowski, J.-L., 2010. On the bias of instantaneous FAPAR estimates in open-canopy forests. Agric. For. Meteorol. 150 (12), 1501–1522.

Widlowski, J.-L., Mio, C., Disney, M., Adams, J., Andredakis, I., Atzberger, C., Brennan, J., Busetto, L., Chelle, M., Ceccherini, G., Colombo, R., Côté, J.-F., Eenmäe, A., Essery, R., Gastellu-Etchegorry, J.P., Gobron, N., Grau, E., Haverd, V., Homolová, L., Huang, H., Hunt, L., Kobayashi, H., Koetz, B., Kuusk, A., Kuusk, J., Lang, M., Lewis, P., Lovell, J.L., Malenovsky, Z., Meroni, M., Morsdorf, F., Möttus, M., Ni-Meister, W., Pinty, B., Rautiainen, M., Schlerf, M., Somers, B., Stuckens, J., Verstraete, M.M., Yang, W., Zhao, F., Zenone, T., 2015. The fourth phase of the radiative transfer model intercomparison (RAMI) exercise: actual canopy scenarios and conformity testing. Remote Sens. Environ. 169, 418–437. https://doi.org/10.1016/j.rse.2015.08.016.

WWW1, 2021. https://land.copernicus.eu/global/gbov.

WWW2, 2021. https://rami-benchmark.jrc.ec.europa.eu/.

Zhang, Z., Zhang, Y., Gobron, N., Frankenberg, C., Wang, S., Li, Z., Zhang, Y., 2020. The potential of satellite FPAR product for GPP estimation: an indirect evaluation using solar-induced chlorophyll fluorescence. Remote Sens. Environ. 240 https://doi.org/10.1016/j.rse.2020.111686.